JOURNAL OF VIROLOGY, June 2005, p. 7146–7161 Vol. 79, No. 11
0022-538X/05/$08.00+0 doi:10.1128/JVI.79.11.7146–7161.2005

Genetic and Cell Biological Characterization of the Vaccinia Virus A30 and G7 Phosphoproteins

Jason Mercer and Paula Traktman*

Department of Microbiology and Molecular Genetics, Medical College of Wisconsin, Milwaukee, Wisconsin 53226

Received 11 January 2005/Accepted 11 February 2005

The vaccinia virus proteins A30 and G7 are known to play essential roles in early morphogenesis, acting prior to the formation of immature virions. Their repression or inactivation results in the accumulation of large virosomes, detached membrane crescents, and empty immature virions. We have undertaken further study of these proteins to place them within the context of the F10 kinase, the A14 membrane protein, and the H5 phosphoprotein, which have been the focus of previous studies within our laboratory. Here we confirm that both A30 and G7 undergo F10 kinase-dependent phosphorylation in vivo and recapitulate that modification of A30 in vitro. Although the detached crescents observed upon loss of A30 or G7 echo those seen upon repression of A14, no interaction between A30/G7 and A14 could be detected. We did, however, determine that the A30 and G7 proteins are unstable during nonpermissive *ts*H5 infections, suggesting that the loss of A30/G7 is the underlying cause for the formation of lacy or curdled virosomes. We also determined that the temperature-sensitive phenotype of the C*ts*11 virus is due to mutations in two codons of the G7L gene. Phenotypic analysis of nonpermissive C*ts*11 infections indicated that these amino acid substitutions compromise G7 function without impairing the stability of either G7 or A30. Utilizing C*ts*11 in conjunction with a rifampin release assay, we determined that G7 acts at multiple stages of virion morphogenesis that can be distinguished both by ultrastructural analysis and by monitoring the phosphorylation status of several viral proteins that undergo F10-mediated phosphorylation.

The morphogenesis of vaccinia virus (VV), the prototypic poxvirus, occurs solely within the cytoplasm of infected cells through a series of stages that are genetically and visually distinct (5, 18). This process begins with the formation of an electron-dense virosome containing the viral proteins to be encapsidated. Crescent-shaped precursors of the virion membrane then develop adjacent to the periphery of the virosome. As these viral crescents enlarge and circularize they envelop a portion of the viroplasm, giving rise to immature virions (IV). IV then acquire an eccentric, electron-dense nucleoid whose appearance is correlated with the encapsidation of the virion genome, a process that we are just beginning to understand (10). Several structural changes, accompanied by a characteristic set of proteolytic processing events, are required for the further transition of nucleoid-containing IV (IVN) into infectious, intracellular mature virions (IMV). IMV represent the majority of infectious particles produced during the course of infection, and have a characteristic brick-shaped appearance with an internal biconcave core (5, 7, 9, 18, 34, 35, 37).

The importance of phosphorylation in the regulation of the vaccinia virus life cycle is underscored by the fact that the vaccinia virus genome encodes two protein kinases (B1 and F10) and a protein phosphatase (H1), all of which are required for virus viability (16, 22, 31, 36). Previous work by our lab and others has placed the F10 kinase at the top of the hierarchy of proteins that play essential roles in the earliest stages of morphogenesis (31, 36). Temperature-sensitive mutants defective in the F10 gene display a very early morphogenesis arrest, prior to virosome condensation or crescent formation. Recent results show that the kinase activity of F10 is essential for its biological function, underscoring the importance of F10-mediated phosphorylation in the biogenesis of both the core and membrane of nascent virions (20, 28).

Several substrates of the F10 kinase have also been shown to play essential roles in early virion morphogenesis. Among them is the H5 protein; during nonpermissive infections with a *ts*H5 mutant, morphogenesis arrests with the formation of "curdled" virosomes and without any evidence of membrane biogenesis (6). The A14 and A17 membrane proteins, which interact with each other, are both phosphorylated in vivo. Repression of either A14 or A17 results in a dramatic inhibition of virion morphogenesis at a stage which is just downstream of the arrest seen when F10 or H5 are defective. In the absence of A17, virosomes become surrounded by a large number of membrane vesicles and/or tubules (23, 38). The absence of A14 leads to the accumulation of large clusters of 20- to 30-nm diameter vesicles and/or tubulovesicular membranes; in addition, a few crescents which appear to be detached from the viroplasmic contacts are also seen (24, 32).

Two additional proteins, A30 and G7, have recently been shown to be involved in the early stages of vaccinia virus morphogenesis. Inducible recombinants have been generated in which either A30 (vA30Li) or G7 (vG7Li) expression can be manipulated experimentally (25, 27, 30) by inclusion or omission of IPTG (isopropyl-β-D-thiogalactopyranoside) from the culture medium. In the absence of either A30 or G7 expression, plaque formation is completely abrogated. Electron microscopic analysis revealed that these aborted infections displayed comparable defects in virion morphogenesis. Crescent

* Corresponding author. Mailing address: Department of Microbiology and Molecular Genetics, Medical College of Wisconsin, 8701 Watertown Plank Rd., BSB-273, Milwaukee, WI 53226. Phone: (414) 456-8253. Fax: (414) 456-6535. E-mail: ptrakt@mcw.edu.

formation was not affected, although further membrane maturation and IV formation was defective. Numerous empty "pseudo-IV" and multiwrapped IV (25, 30) were seen. When nonpermissive infections with either a temperature-sensitive mutant defective in A30 (D*ts*46) or the inducible A30 recombinant virus were performed at 39.7°C, the virosomes appeared "lacy" (27, 30). The authors of these studies concluded that A30 and G7 are required for the recruitment and/or attachment of viral crescents to the viroplasm and the subsequent formation of immature virions. In addition, A30 and G7 were shown to interact with one another and to be mutually dependent upon each other for stability (25). A30 and G7 were also shown to complex with and stabilize the viral F10 kinase, which was in turn found to be necessary for the in vivo phosphorylation of A30 (29).

Several of the phenotypic characteristics observed upon repression of A30 or G7 were reminiscent of those seen upon repression of the A14 membrane protein or mutation of the H5 core protein: a defect in crescent/virosome juxtaposition and the presence of "curdled" virosomes. These coincident phenotypes prompted us to investigate the possible genetic and/or functional links between the A30, G7, H5, and A14 proteins during the course of VV morphogenesis. We present these studies here, as well as our analysis of the temperature-sensitive mutant C*ts*11, which we have determined to encode a defective G7 allele. These studies confirm that there are functional interactions between the A30, G7, and H5 proteins and reveal that the G7 phosphoprotein functions during several stages of virion maturation.

MATERIALS AND METHODS

Materials. Restriction endonucleases, T4 DNA ligase, calf intestinal phosphatase, pancreatic RNase, *Taq* polymerase, and DNA molecular weight standards were purchased from Invitrogen (Carlsbad, Calif.). [^{32}P]orthophosphate and [^{35}S]methionine were obtained from Dupont/New England Nuclear Corp. (Boston, Mass.). Lipofectamine Plus reagent was purchased from Invitrogen life Technologies (Carlsbad, Calif.), and Endofree Plasmid Maxi kits were from Qiagen (Valencia, Calif.). DNA oligonucleotides were synthesized by IDT (Coralville, Iowa). Thin-layer chromatography plates were purchased from EM Separations, Inc. (Gibbstown, N.J.), and constant boiling HCl was from Pierce (Rockford, Ill.).

Cells and viruses. Monolayers of BSC40 primate cells were maintained in Dulbecco modified Eagle medium (DMEM; Invitrogen Life Technologies) containing 5% fetal bovine serum at 37°C. Wild-type vaccinia virus (strain WR), v*ind*A13 (33), *ts*H5-4 (6), v*ind*H1 (16), C*ts*11 (the present study [kindly supplied by Richard Condit]) (14), and v*ind*F18 (vRO11K [39]; kindly provided by Bernard Moss, NIH, Bethesda, Md.) were used where indicated. All viral stocks were prepared by ultracentrifugation of cytoplasmic lysates of infected BSC40 cells or L cells (for wild type [wt]) through 36% sucrose; in some instances, virions were further purified by banding on 25 to 40% sucrose gradients (16). For infections with temperature-sensitive mutants, 31.5 and 39.7°C were used as the permissive and nonpermissive temperatures, respectively.

Preparation of anti-A30 and anti-G7 sera. (i) Construction of pATH:A30. The A30 open reading frame (ORF) was amplified by PCR by using genomic DNA as the template. The upstream primer (5′-AC**GGATCC**ATGGAAGACCTTAA CGA-3′) introduced a BamHI site (in boldface) upstream of the initiating ATG (underlined). The downstream primer (5′-CC**GGTACC**TCAACGACGATTGA ATT-3′) introduced a KpnI site (in boldface) immediately downstream of the translation stop site (underlined). The 234-bp PCR product was then digested with BamHI and KpnI and inserted into pATH23 vector DNA (13) that had been previously digested with the same enzymes and treated with calf intestinal alkaline phosphatase (CIP). The resulting plasmid places the A30 gene downstream of and in frame with the *E. coli trpE* gene.

(ii) Construction of pATH:G7. The G7 ORF was amplified by PCR by using vaccinia virus genomic DNA as the template. The upstream primer (5′-CGC**G GATCC**ATGGCTGCAGAACAGCGTCG-3′) places a BamHI site (in boldface) upstream of the initiating ATG (underlined). The downstream primer (5′-CGC**GGATCC**TTAACATTTTGGCAAATTG-3′) introduces a BamHI site (in boldface) downstream of the translational stop site (underlined). The 1,116-bp PCR product was digested with BamHI and ligated with pATH-1 vector DNA that had been treated with BamHI and CIP (13). The resultant plasmids were screened for proper orientation of the insert; the plasmid selected placed the G7 gene downstream of and in frame with the *Escherichia coli trpE* gene.

(iii) Expression of trpE:A30 and trpE:G7 antigens. *E. coli* transformants containing pATH:A30 or pATH:G7 directed the inducible synthesis of 43- and 76-kDa fusion proteins that comprised 34 kDa of *E. coli* trpE and either 9 kDa of A30 or 42 kDa of G7, respectively. These fusion proteins were excised from copper chloride-stained sodium dodecyl sulfate (SDS)-polyacrylamide gels and used for the immunization of rabbits. In each case, the specificity of the resultant polyclonal antisera was confirmed by both immunoblot and immunoprecipitation analyses.

Immunodetection analysis. Cell lysates or immunoprecipitates were resolved by SDS-polyacrylamide gel electrophoresis (PAGE) and transferred to nitrocellulose (Schleicher & Schuell, Keene, N.H.) filters in CAPS transfer buffer (10 mM CAPS {3-[(cyclohexylamino)-1-propane-sulfonic acid]} in 10% methanol; pH 11.3). Filters were probed with the indicated antisera directed against A30, G7, or H5 and then with horseradish peroxidase-conjugated secondary antibody (Bio-Rad, Richmond, Calif.). Immunoreactive species were visualized after development with enhanced chemiluminescence reagents (Pierce, Rockford, Ill.).

Metabolic labeling. (i) Metabolic labeling with [^{35}S]methionine. Monolayers of BSC40 cells were infected at a multiplicity of infection (MOI) of 5 with the indicated virus. At 6 h postinfection (hpi) the cultures were rinsed with methionine-free DMEM (ICN-FLOW, Costa Mesa, Calif.) supplemented with L-glutamine and fed with the same medium containing 100 μCi of [^{35}S]methionine (EXPRESS label; NEN-Dupont) per ml. Cells were labeled for a total of 3 h and prepared for immunoprecipitation analysis as follows. Cells were rinsed with phosphate-buffered saline and lysed in 1× phospho-lysis buffer (0.1 M $NaPO_4$ [pH 7.4], 0.1 M NaCl, 1% Triton X-100, 0.1% SDS, 0.5% sodium deoxycholate). Lysates were clarified by centrifugation and incubated with primary serum, followed by protein A-Sepharose (Sigma); immunoprecipitates were then retrieved, washed thoroughly, and analyzed by SDS-PAGE and autoradiography.

(ii) Labeling with $^{32}PP_i$. Infected monolayers were incubated with phosphate-free DMEM (ICN-Flow) supplemented with phosphate-free 5% fetal bovine serum (prepared by dialysis against Tris-buffered saline [25 mM Tris-HCl [pH 7.4], 136 mM NaCl, 2.7 mM KCl]) and 100 μCi of ^{32}PPi per ml. Labeling was performed from 6 to 9 hpi, and cells were then harvested as described above for immunoprecipitation analyses. When appropriate, a cocktail of phosphatase inhibitors (1 mM sodium orthovanadate, 1 mM sodium fluoride, and 40 mM β-glycerol phosphate) was added to the 1× phospho-lysis buffer.

Pulse-chase analysis. Duplicate sets of confluent 60-mm dishes were infected with the indicated virus at an MOI of 2; one set was incubated at the permissive temperature (31.5°C), the second set was incubated at the nonpermissive temperature (39.7°). At 6 hpi cells were labeled with [^{35}S]methionine as described above. After a 15-min pulse-labeling, one culture was harvested and designated as the "zero time" sample. The remaining dishes were rinsed 1× with complete medium (containing cold methionine) and returned to the incubator for chase periods of 15 to 360 min, as indicated. All samples were then subjected to immunoprecipitation analyses.

One-dimensional phosphoamino acid analysis. One-dimensional phosphoamino acid analysis (PAA) was performed as previously described (32). Briefly, ^{32}P-labeled A30 and G7 were immunoprecipitated from metabolically labeled wt-infected extracts. Immunoprecipitates were resolved by SDS-PAGE and transferred electrophoretically to Immobilon P; the appropriate radiolabeled bands were excised from the filter for further processing. After hydrolysis in situ, the samples were precipitated, mixed with phosphoamino acid markers (20 nmol each), and spotted onto thin-layer cellulose F chromatography plates. Phosphoamino acids were resolved by electrophoresis on a Hunter thin-layer electrophoresis system, model HTLE 7000, at 1,800 V for 30 min in pyridine-glacial acetic acid-water (1:10:189). Markers were visualized by ninhydrin staining, followed by development at 65°C; the samples were then visualized by autoradiography.

Preparation of recombinant N′HIS-A30 and C′HIS-G7. Plasmids encoding His-tagged versions of both A30 and G7 were constructed for the purpose of bacterial expression and purification.

(i) N′HIS-A30. The upstream primer (5′-GGAATTC**CAT**ATGGAAGACCT TAACG-3′), which inserts an NdeI site (in boldface) overlapping the translational start site (underlined) and the downstream primer (5′-CGC**GGATCC**TC AACGACGATTGAATTCT-3′), which contains a BamHI site (in boldface) downstream of the translational stop site (underlined), were used to amplify the

A30 ORF utilizing VV genomic DNA as the template. The PCR product was digested with the appropriate enzymes and ligated to pET-16b (Novagen, Madison, Wis.) DNA that had been previously digested with the appropriate enzymes and treated with CIP. This plasmid placed the A30 ORF under the regulation of an inducible T7 promoter, downstream of and in frame with a 10×-His tag. After expression in *E. coli* BL21(DE3) transformants, the N′-tagged A30 protein was affinity purified on Ni-NTA agarose (Qiagen, Valencia, Calif.).

(ii) C′HIS-G7. The upstream primer (5′-GGATCC**CC**ATG**G**ACATGATGC TTAT-3′), which inserts an NcoI site (in boldface) overlapping the translational start site (underlined) of G7, and the downstream primer (5′-CCG**CTCGAG**A CATTTTGGCAAATTG-3′), which contains a XhoI site (in boldface), were used to amplify a copy of the G7 ORF lacking the translational stop codon. After digestion with NcoI and XhoI, the insert was ligated into pET-23d DNA that had been similarly digested and treated with CIP. The final plasmid encoded a T7-inducible G7-10×-His fusion protein. Recombinant C′-tagged G7 was purified from *E. coli* BL21(DE3) transformants as described above.

In vitro kinase reactions. Recombinant His-A30 and His-G7 proteins were evaluated for their ability to serve as substrates for the VV-encoded F10 and B1 kinases. A total of 150 ng of A30 or 450 ng of G7 were incubated in 25-μl reactions containing 25 ng of recombinant 3×-FLAG-F10 (20) or 50 ng of recombinant His-B1 (unpublished data), 50 mM Tris (pH 7.5), 1 mM dithiothreitol, 5 μM rATP, and 10 μCi of [γ-^{32}P]ATP (3,000 Ci/mmol). Reactions were allowed to proceed for 30 min at 25°C. Control reactions for the F10 and B1 kinases contained 2.5 μg of myelin basic protein (MBP) or casein, respectively. Samples were subjected to fractionation by SDS-PAGE, and the phosphorylated products were visualized by autoradiography.

Marker rescue assay. Confluent monolayers of BSC40 cells were infected with C*ts*11 at an MOI of 0.03 at the permissive temperature (31.5°C). At 3 hpi, 5 μg of pTM1 (empty vector), pBR322-*Hin*dIIIG, pTM1-G7, pTM1-G7$_{P113S}$, pTM1-G7$_{A135V}$, or pTM1-G7$_{P113S;A135V}$ DNA which had been previously linearized with ScaI were applied to cells as $CaPO_4$ precipitates. Cultures were then shifted to the nonpermissive temperature; at 48 hpi, cells were harvested, and the viral yield was determined by titration on BSC40 cells. Experiments were performed in triplicate, and the titers were averaged.

Marker rescue analyses utilizing G7 cleavage mutants. To determine whether G7 alleles in which one or both of the proteolytic cleavage sites (AG ↓ X) had been inactivated (AAX) could support virus viability, marker rescue of C*ts*11 was performed as described above with plasmids encoding the following alleles: pTM1-G7, pTM1-G7$_{G183A}$, pTM1-G7$_{G238A}$, and pTM1-G7$_{G183A;G238A}$. Temperature-insensitive plaques that formed at 39.7°C were purified and then assessed for their genotype at the relevant codons. In each case, the nucleotide substitutions alter a restriction endonuclease cleavage site, either an AluI site (AGCT) at position 183 or a NaeI site (GCCGGC) at position 238, enabling the wt (AGX) and mutant (AAX) alleles to be rapidly differentiated. For the construction of AGX cleavage mutants, targeted mutations within the G7 gene were generated by using a previously described overlap PCR strategy (17). VV genomic DNA was used as the template for the initial round of PCRs. In the first round of PCR, two reactions were performed. Reaction B used an upstream primer (5′-GGATCC**CC**ATG**G**ACATGATGCTTAT-3′), which inserts an NcoI site overlapping the translational start site (underlined) of G7 in conjunction with one of two mutation-encoding primers: primer 183 "AAX"-b (5′-CAGAA AATGCCGCTACTATAATAGG-3′) or 238 "AAX"-b (5′-TTTTCAAGGCGG CTATATATTCTGC-3′). Reaction C used a downstream primer (5′-CGC**GGA TCC**TTAACATTTTGGCAAATTG-3′), which inserts a BamHI site (in boldface) downstream of the G7 translational stop site (underlined), together with either 183 "AAX"-c (5′-GTAGCGTGCATTTTCTGGTAAAGAAC-3′) or 238 "AAX"-c (5′-TATAGCCGCCTTGAAAATAGAAGAGATTG-3′). Portions (1 μl) of the products generated in the corresponding B and C reactions were used together as the template for the second round of PCR, which used only the upstream and downstream primers. In the case of G7$_{G183A;G238A}$, the final 183 "AAX" PCR product served as the template for the subsequent 238 "AAX" mutagenesis. Each of the final products was subjected to analytic restriction digestion with AluI and/or NaeI to confirm the loss of the appropriate restriction site. The inserts were then digested with NcoI and BamHI and ligated to previously digested and CIP-treated pTM1 vector DNA. The sequence of all constructs were confirmed by automated DNA sequence analysis.

RIF release of C*ts*11. Dishes (60 mm) of BSC40 cells were infected with wt virus or C*ts*11 virus in quadruplicate (MOI of 5) in the presence of 100 μg of rifampin (RIF)/ml. Infections were allowed to proceed at 31.5°C for 12 h, at which time two plates from each set of infections were shifted to 39.7°C, while the other two of each set were maintained at 31.5°C. At this time, one plate from each set was subjected to washing and refeeding to remove rifampin, while the other plate was maintained in the presence of drug. The infection was then allowed to proceed for an additional 7 h. Cells were then harvested, and the viral yield was determined by plaque assay. The status of the G7 protein was monitored by immunoblot analysis.

Transmission EM. Cells were prepared for electron microscopy (EM) as previously described (12, 31). (i) For C*ts*11, 60-mm dishes of BSC40 cells were infected with C*ts*11 at an MOI of 2 at 31.5°C or 39.7°C. At 17 hpi the cells were rinsed with cold phosphate-buffered saline (PBS) and fixed in situ with 1% glutaraldehyde-PBS for 1 h on ice. Samples were then subjected to postfixation with osmium tetroxide, dehydration, and embedding as previously described (31). (ii) For C*ts*11 rifampin release, cells were infected and treated as described above for C*ts*11 rifampin release, with the following exceptions. At 12 hpi one set (wt and C*ts*11) of plates was harvested for EM (no RIF release); the other set was washed and refed with medium lacking rifampin (Shift/RIF release) and shifted to 39.7°C for an additional 3 h of incubation prior to being harvested and processed for EM.

Construction of pTM1-3XFLAG-A30, pTM1-G,7 and pTM1-*ts*G7. (i) The various pTM1 constructs were generated by PCR utilizing wt or C*ts*11 genomic DNA as a template. The 5′ primer 5′-CGCGGATC**CAT**ATGGAAGACCTTA ACG-3′ inserts an NdeI site upstream of the translational start site (underlined) of A30. The downstream primer 5′-CGC**GGATCC**TCAACGACGATTGAAT T-3′ introduces a BamHI site (in boldface) downstream of the A30 translational stop site (underlined). The A30 PCR product was digested with the appropriate enzymes and ligated to pTM1-3XFLAG DNA (20) that had been similarly digested and treated with CIP. (ii) The 5′ primer 5′-GGATCC**CC**ATG**G**ACA TGATGCTTAT-3′ inserts an NcoI site overlapping the translational start site (underlined) of G7. The downstream primer (5′-CGC**GGATCC**TTAACATTTT GGCAAATTG-3′) introduces a BamHI site (in boldface) downstream of the G7 translational stop site (underlined). PCR products were digested with the appropriate enzymes and ligated to pTM1 plasmid DNA that had been similarly digested and treated with CIP (8). The A30, G7, and *ts*G7 plasmids were purified from *E. coli* transformants and their identity and fidelity was verified by automated DNA sequencing.

IVTT of A30, G7, or *ts*G7. The TnT system from Promega (Madison, Wis.) was used for the in vitro transcription and translation (IVTT) of pTM1-3XFLAG-A30, pTM1-G7, and pTM1-*ts*G7. A total of 50-μl reactions were programmed with these plasmids, either singly or in pairs, and incubated at 30°C for 90 min in the presence of 20 μCi [^{35}S]methionine. A small sample was removed from each reaction, and the remainder was diluted sixfold into TnT-I.P. buffer (50 mM Tris [pH 7.4], 150 mM NaCl, 0.05% Triton X-100) and divided into three aliquots that were subjected to immunoprecipitation with either α-FLAG M2 monoclonal antibody (Sigma-Aldrich, St. Louis, Mo.) or α-A30 or α-G7 sera. Immunoprecipitations were carried out as described above; radiolabeled proteins were resolved by SDS-PAGE and visualized by autoradiography.

Preparation of figures. Alignments were performed by using the CLUSTAL V method and Lasergene software (DNASTAR, Inc., Madison, Wis.) utilizing sequences retrieved from the Poxvirus Bioinformatics Resource Center (http://www.poxvirus.org). Original data were scanned on an Epson expression 1680 scanner (Epson, Long Beach, Calif.) and adjusted with Adobe Photoshop software (Adobe Systems, Inc., San Jose, Calif.). Graphs were prepared in Sigma plot (SPSS, Chicago, Ill.), and final figures were prepared with Canvas software (Deneba Systems, Inc., Miami, Fla.).

RESULTS

Investigation of possible A30/G7/A14 interactions utilizing immunoprecipitation analysis. Ultrastructural analyses have suggested that the association of nascent crescent membranes with viroplasm is compromised when the A14 (24, 32), A30 (27, 30), or G7 (25) proteins are repressed during the course of viral infection. A physical interaction between the A30 and G7 proteins has also been demonstrated (25). Because of our prior interest in the role of the A14 membrane protein, we were interested in probing for interactions between A14 and either A30 or G7. Polyclonal sera were generated to the A30 and G7 proteins; both sera were found to be effective in immunoprecipitation and immunoblot assays. The nascent A30 protein exhibited an apparent molecular mass of ~9 kDa (Fig. 1A, α-A30); the G7 protein exhibited an apparent molecular mass of ~42 kDa (Fig. 1A, α-G7). In these analyses of wt-infected

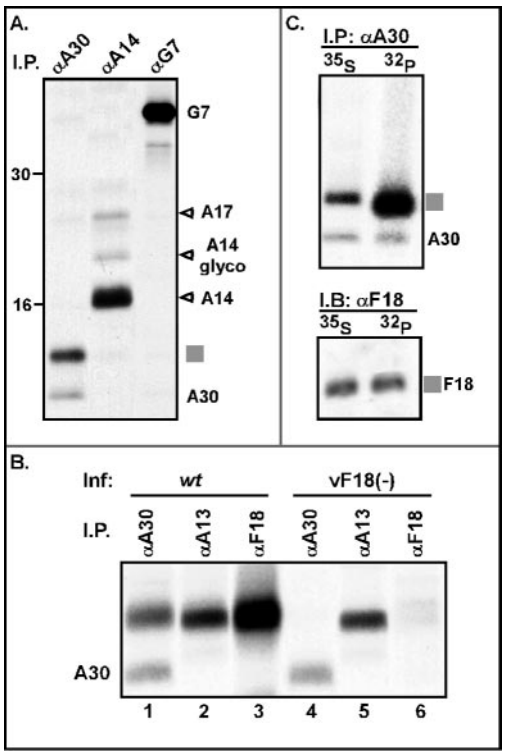

FIG. 1. Immunoprecipitation analysis of G7 and A30 expression; A30 and G7 do not coprecipitate, but A30 associates with the F18 protein. (A) Immunoprecipitation analysis of nascent A30, G7, and A14. BSC40 cells infected with wt virus at an MOI of 5 were labeled with [^{35}S]methionine from 6 to 9 hpi. Lysates were subjected to immunoprecipitation analysis with α-A30, α-G7, and α-A14 sera. The precipitates were resolved by SDS-PAGE and visualized by autoradiography. Each serum retrieved the cognate protein; in addition, the α-A30 precipitate contained a strongly labeled species of ~11 kDa (■), and the α-A14 precipitate contained the ~21-kDa A17 protein, as well as A14 and a small amount of glycosylated A14 (A14 glyco). No interaction between A30 and G7 was detected. The precipitated proteins are identified at the right; molecular markers are shown at the left, with their masses given in kilodaltons. (B) The 11-kDa protein coprecipitating with A30 migrates with A13 and F18 and is not retrieved when F18 expression is repressed. Cells were infected with either wt virus (lanes 1 to 3) or the inducible F18 recombinant in the absence of IPTG (vF18[−], lanes 4 to 6). Cells were metabolically labeled and subjected to immunoprecipitation as described for panel A. (C) The 11-kDa protein that coprecipitates with A30 is the viral F18 protein. Cells infected with wt virus (as described in panel A) were pulse-labeled with either [^{35}S]methionine or [^{32}P]Pi and subjected to immunoprecipitation with α-A30. The immunoprecipitates were resolved in duplicate by SDS-PAGE; one set was visualized directly by autoradiography (I.P.; top), and the second was subjected to immunoblot analysis with α-F18 serum (I.B.; bottom).

cells, we did not observe any physical interactions between the A14, A30, or G7 proteins (Fig. 1A). As an internal control we monitored the coprecipitation of A17 with A14; retrieval of this known binding partner of A14 was consistently observed (Fig. 1A, α-A14). Radiolabeled A30 protein was retrieved by the α-A30 serum when lysates were prepared from cells metabolically labeled with either [^{35}S]methionine or ^{32}PPi (Fig. 1A and C), confirming that the A30 protein is phosphorylated in vivo. In our α-A30 precipitations, we consistently observed a second protein of ~11 kDa (Fig. 1A to C; ■ 11kDa), as well as the ~9-kDa A30 protein. This 11-kDa protein was shown to be phosphorylated (Fig. 1C, top panel) and to possess an electrophoretic migration indistinguishable from that of the A13 membrane protein or the abundant F18 core protein (Fig. 1B, lanes 1 to 3). Retrieval of the 11-kDa protein was dependent upon expression of the F18 protein, as shown by analysis of lysates prepared from cells infected with a recombinant virus in which F18 is repressed when IPTG is omitted from the culture medium (Fig. 1B, lanes 4 to 6) (39). Confirmation that the coprecipitating protein was indeed F18 was obtained by immunoblot analysis of the resolved immunoprecipitates (Fig. 1C, bottom panel). The presence of the F18 protein in the α-A30 precipitates does not appear to be due to cross-reactivity of the serum, since the α-A30 serum does not recognize the F18 protein in immunoblot analyses (not shown). It should also be noted that, although F18 is a highly abundant protein (11), it is not observed as a contaminant in all precipitations, as shown by the absence of an ~11-kDa protein in the α-G7 and α-A14 precipitates (see Fig. 1A). Whether this observed interaction between the A30 and F18 proteins has any biological significance remains to be determined.

A30 and G7 are phosphorylated in vivo, and A30 is a substrate for viral kinases in vitro. The data presented in Fig. 1C showed that the A30 protein was phosphorylated during wt infections. To determine whether the phosphorylation of A30 was modulated by the viral F10 kinase and H1 phosphatase in vivo, we examined the profile of radiolabeled A30 during a variety of infections: wt virus, *ts*28 at 39.7°C, (defective in the F10 kinase), and v*ind*H1-IPTG (H1 expression repressed). As shown in Fig. 2A, the radiolabeling of A30 was abrogated when F10 was compromised (lane 2, upper panel) and enhanced when H1 was repressed (lane 3, upper panel). Immunoblot analyses of the lysates confirmed that A30 was stable under all conditions, and that A30 appeared as a double (arrowheads, lower panel) in wt and H1-deficient infections. The upper band of this doublet (filled arrowhead, lower panel) was absent when F10 was inactive and of greater intensity when H1 was absent, indicating that its presence correlated with the phosphorylation of A30. Phosphoamino acid analysis of the precipitated, ^{32}P-labeled A30 indicated that the modification occurred solely on serine residues during wt infections (right panel), H1-deficient infections (not shown), as well as in vitro (Fig. 2C) (data not shown). We performed a comparable analysis of the G7 protein, as shown in Fig. 2B. Once again, we found that the G7 protein was ^{32}P-labeled during wt infections and that this phosphorylation was absent when the F10 kinase was inactive (upper panel, lane 2, *ts*28 [−] infections) and augmented when the H1 phosphatase was repressed (upper panel, lane 3, v*ind*H1 [−] infections). Immunoblot analysis confirmed the accumulation of G7 during all of these infections (lower panel), although a reduction in protein levels was noted in the lysate prepared from the *ts*28 infection (lower panel, lane 2). The phosphorylation of G7 was also shown to affect only serine residues (right panel). Cumulatively, these results indicated that both A30 and G7 are phosphorylated on serine residues in vivo and that the regulated execution of this modification is genetically dependent upon both the vaccinia virus encoded F10 kinase and H1 phosphatase.

Our observation that the phosphorylation of A30 and G7 in vivo was abrogated in *ts*28 suggested either that the F10 kinase itself was responsible for phosphorylating the two proteins

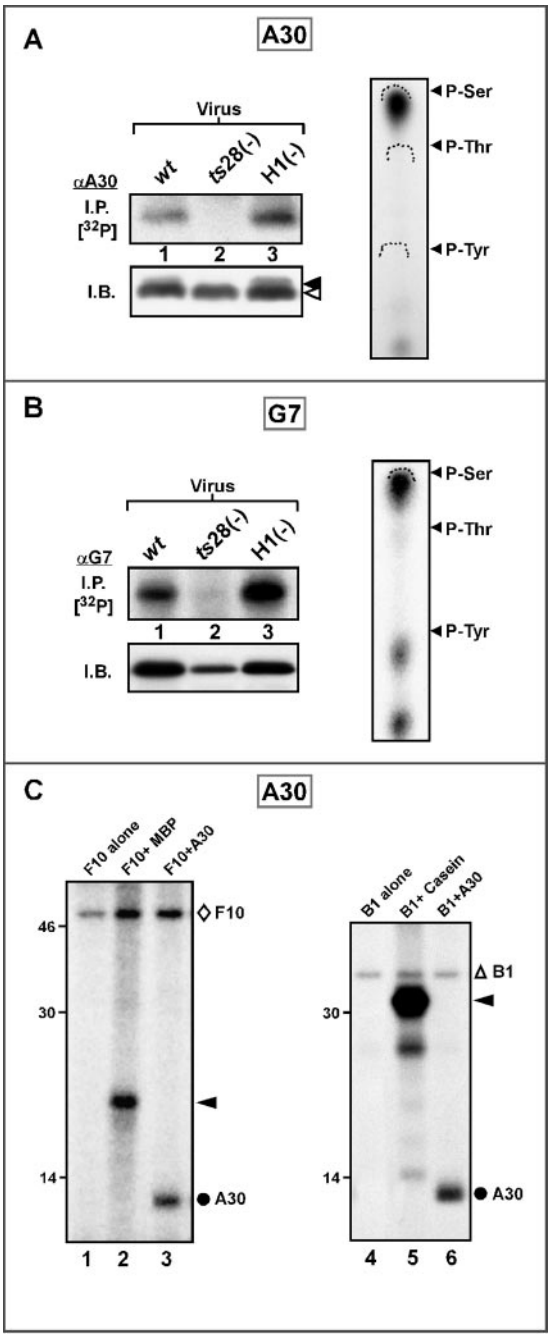

FIG. 2. A30 and G7 are phosphorylated on serine residues in vivo in an F10-dependent manner; A30 is a substrate for the F10 and B1 kinases in vitro (A) Phosphorylation of the A30 protein in vivo. BSC40 cells were infected with the indicated viruses {wt, *ts*28 at 39.7°C [*ts*F10(−)], or v*ind*H1 in the absence of IPTG [H1(−)]} at an MOI of 5 and pulse-labeled with ^{32}PPi from 6 to 9 hpi; lysates were subjected to immunoprecipitation analysis with the α-A30 serum. The immunoprecipitates and lysates were resolved by SDS-PAGE; the latter were visualized by autoradiography, and the former were subjected to immunoblot analysis with the α-A30 serum (I.B.). Filled and empty triangles mark the differential migration of phosphorylated and unphosphorylated A30 (A30 I.B.) An additional sample of ^{32}P-A30 was retrieved by immunoprecipitation from wt-infected lysates and subjected to phosphoamino acid analysis (PAA). The positions to which phosphoamino acid markers (P-ser, P-thr, and P-tyr) migrated are indicated by the wickets; the radiolabeled phosphoamino acids derived from A30 were visualized by autoradiography. (B) Phosphorylation of the G7 protein in vivo. Phosphorylation of the G7 protein was analyzed exactly as described above for A30 in panel A, except that a polyclonal α-G7 serum was used. (C) Recombinant N′his-A30 is a substrate for both the F10 and B1 kinases in vitro. In the left panel, purified F10 kinase was assayed alone (lane 1), in the presence of the generic substrate MBP (lane 2), or in the presence of recombinant N′his-A30 (lane 3). All reactions were performed at 25°C for 30 min in the presence of [γ-^{32}P]ATP. Autophosphorylation of F10 (△), phosphorylation of MBP (◀), and phosphorylation of A30 (●) were readily observed. In the right panel, recombinant B1 kinase was assayed alone (lane 1), in the presence of the generic substrate casein (lane 2), or in the presence of N′his-A30 (lane 6). Autophosphorylation of B1 (△), phosphorylation of casein (◀), and phosphorylation of A30 (●) were readily observed. The electrophoretic migration of molecular weight markers, with their masses indicated in kilodaltons, is shown at the left of each autoradiograph.

directly or that phosphorylation could not occur in the absence of ongoing viral morphogenesis. In an attempt to distinguish between these possibilities, we monitored the ability of recombinant N′his-A30 and N′his-G7 to serve as substrates for purified 3XFLAG-F10 kinase in vitro. As shown in the left panel of Fig. 2C, autophosphorylation of F10 (◇, lanes 1 to 3), phosphorylation of the generic substrate MBP (◀, lane 2) and phosphorylation of A30 were easily observed (●, lane 3). Despite numerous attempts, we were unable to observe any F10-mediated phosphorylation of recombinant G7 protein (not shown), either alone or in the presence of A30, with which G7 has been shown to interact directly. VV also encodes the B1 kinase, which is expressed early during infection and is present throughout the duration of the infectious cycle (1, 15, 21, 22). A role for B1 in the phosphorylation of A30 and G7 cannot easily be monitored in vivo, because temperature-sensitive mutants encoding a defective B1 kinase are defective in DNA synthesis and hence late proteins are not expressed at the nonpermissive temperature. We therefore tested the ability of recombinant B1 kinase to phosphorylate A30 and G7 in vitro. As shown in the right panel of Fig. 2C, we could readily observe autophosphorylation of B1 (△, lanes 4 to 6), phosphorylation of the generic substrate casein (◀, lane 5), and phosphorylation of A30 (●, lane 6). Again, we did not observe any B1-mediated phosphorylation of G7 (not shown). These findings suggest that either the phosphorylation of G7 in vivo may be mediated by a cellular kinase or that phosphorylation by one or both of the viral kinases only occurs in the context of ongoing morphogenesis. In contrast, A30 can be phosphorylated in vitro by either viral kinase, but the presence of B1 alone in vivo is not sufficient for modification of A30. It may be that only F10 can phosphorylate A30 in vivo, or again that phosphorylation can only occur in the context of ongoing morphogenesis.

A30 and G7 proteins are unstable during nonpermissive *ts*H5-4 infections. At 39.7°C, inactivation or repression of the A30 protein [vA30Li(−) and D*ts*46 (27, 30)] leads to the formation of aberrant virosomes referred to as "lacy"; these virosomes closely resemble those noted during nonpermissive infections performed with the *ts*H5-4 virus and referred to as "curdled" (6). The constitutively expressed and abundant H5 protein has been shown to serve as a substrate for the viral B1 kinase (2), to associate with the late transcriptional machinery (3), and to be involved in viral morphogenesis: nonpermissive

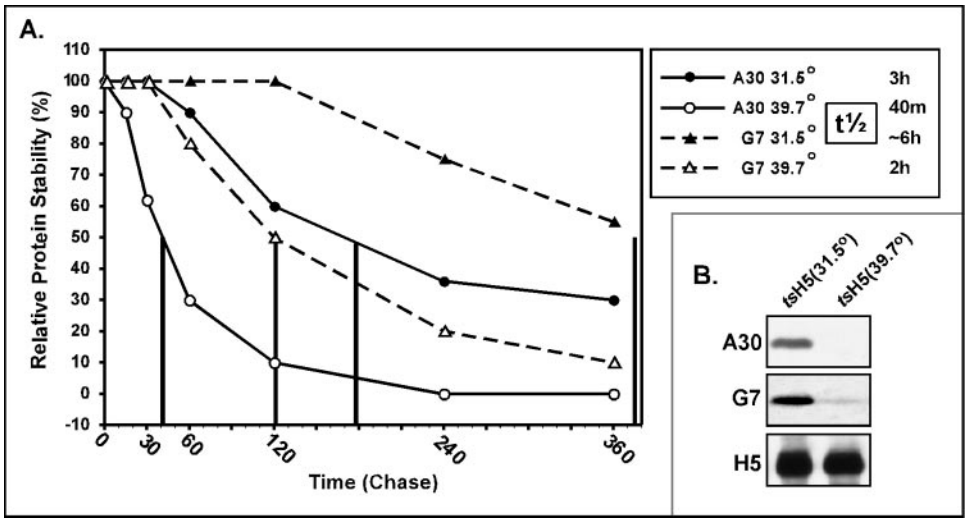

FIG. 3. The stability of A30 and G7 are dependent upon a functional H5 protein. (A) Determination of the $t_{1/2}$ of A30 and G7 during permissive and nonpermissive *ts*H5 infections. Multiple dishes of BSC40 cells were infected with *ts*H5-4 (MOI 5) at both 31.5 and 39.7°C. At 6 hpi all dishes were pulse-labeled with [^{35}S]methionine for 15 min. One dish from each temperature set was harvested immediately (pulse, 0); the remaining dishes were washed and refed with complete medium and subjected to further incubations of 30, 60, 120, 240, and 360 min (chase). Lysates were prepared and subjected to immunoprecipitation analysis with α-A30 and α-G7 sera; resolved immunoprecipitates were visualized by fluorography. The levels of A30 and G7 remaining after each chase period were normalized to the level found in the pulse sample and are shown graphically. The vertical lines illustrate the times at which 50% of each protein remains; these extrapolated $t_{1/2}$ values are shown in the box at the right of the graph. (B) Immunoblot analysis of steady-state levels of A30, G7, and H5 during *ts*H5 infections. Aliquots of the *ts*H5-infected "360-min" chase cultures described above, i.e., harvested at 9.25 hpi, were subjected to immunoblot analysis with α-A30, α-G7, and α-H5 sera. A temperature-dependent loss of A30 and G7, but not H5, was observed.

*ts*H5-4 infections show no defect in gene expression but show an arrest in morphogenesis that occurs prior to any evidence of membrane biogenesis (6). To investigate the possibility of a functional or genetic link between H5, A30, and G7, we investigated the status of A30 and G7 during nonpermissive *ts*H5-4 infections. Previous reports had indicated that the stability of A30 and G7 was dependent upon one another (25); we wanted to determine whether their stability was dependent upon a functional H5 protein as well. Pulse-chase analysis of A30 and G7 in cells infected with *ts*H5-4 enabled us to determine that the half-lives of the A30 and G7 proteins were 3 and ~6 h, respectively, at the permissive temperature (Fig. 3A). Under nonpermissive conditions the half-lives of both proteins were significantly reduced, with the $t_{1/2}$ of A30 decreasing ~4.5-fold to 40 min and the $t_{1/2}$ of G7 decreasing ~3-fold to 2 h. Immunoblot analysis of extracts prepared at 6 hpi reinforced the conclusion that A30 and G7 are unstable during nonpermissive *ts*H5-4 infections (Fig. 3B). As an internal control, the half-life of the H5 protein was assessed as well and found to be unchanged (not shown); the stability of the H5 protein during these infections has been reported previously (6) and is confirmed by the immunoblot shown in Fig. 3B. Immunoblot analysis was also used to monitor numerous other late proteins, and in no other case was protein accumulation shown to be altered during the nonpermissive *ts*H5-4 infection (not shown). To assess whether the apparent dependence of A30 and G7 stability on H5 was reciprocal, the steady-state level of the H5 protein was monitored during permissive and nonpermissive infections with temperature-sensitive viruses encoding lesions in A30 (D*ts*46) or G7 (C*ts*11, see below); the accumulation of the H5 protein was equivalent in all cases (data not shown and Fig. 10). Cumulatively, these data suggest that it is the loss of the A30 and/or G7 proteins that underlies the aberrant virosome morphology seen during nonpermissive *ts*H5-4 infections (6).

The temperature sensitivity of C*ts*11 is due to two independent amino acid substitutions within the G7 gene. During the course of these studies, we noted that a temperature-sensitive virus belonging to the Condit collection, C*ts*11, was tentatively assigned to the genomic region comprising the G6R, G7L, and G8R genes (14). To determine whether the temperature sensitivity of this virus was due to a mutation in G7L, we performed marker rescue analyses to identify which DNA sequences could generate temperature-insensitive virus upon homologous recombination into the C*ts*11 genome. Linearized plasmids containing either the complete HindIII G fragment of the VV genome or the G7L ORF alone increased the titer of temperature-insensitive virus emerging from C*ts*11 infections by >4 orders of magnitude, whereas linearized vector DNA had no effect (Fig. 4A, rows 1 to 3). The sequence of the G7L ORF encoded by the C*ts*11 genome was determined for two plaque-purified isolates; two mutations which resulted in Pro^{113}→Ser and Ala^{135}→Val substitutions were found in each case (Fig. 4B). As shown by an alignment of the predicted protein sequences of the G7 homologs encoded by multiple poxviruses, including those closely related to vaccinia virus (camelpox, variola, and monkeypox viruses), as well as more distant relatives (myxoma and fowlpox viruses), these substitutions affect highly conserved or invariant residues. In order to assess the contribution of the individual mutations to the temperature sensitivity of C*ts*11, further marker rescue analysis was performed with G7 alleles containing one or both of the mutations. Only the fully wt allele was competent to generate temperature-insensitive virus (Fig. 4A, rows 3 to 6). These

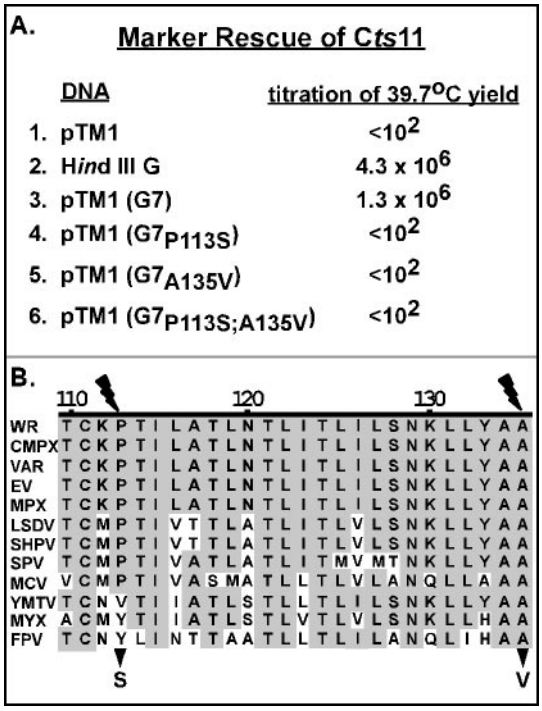

FIG. 4. The temperature-sensitive phenotype of C*ts*11 is due to mutations in the G7R gene. (A) The G7 gene can rescue the temperature-sensitive phenotype of C*ts*11. BCS40 cells were infected with C*ts*11 (MOI = 0.03) at 31.5°C; at 3 hpi, cultures were transfected individually with the indicated linearized DNA constructs and shifted to the nonpermissive temperature (39.7°C). At 48 h, cultures were harvested, and the yield of temperature-insensitive virus was determined by titration at 39.7°C. The value shown represents the average of triplicate experiments. Only the HindIIIG fragment and pTM1(G7) were able to restore the production of temperature-insensitive virus. (B) Comparative sequence alignment of the region surrounding the lesions within the G7R ORF. An alignment of residues 110 to 135 of the G7 homologs encoded by various poxviruses is shown; residues that match the vaccinia virus WR sequence are shaded. The lightning bolts indicate the position of the temperature-sensitive mutations, with the amino acid substitutions shown beneath the arrowhead. Abbreviations: VV WR strain (WR), camelpox virus (CMPX), variola virus (VAR), ectromelia virus (EV), monkeypox virus (MPX), lumpy skin virus (LSDV), sheeppox virus (SHPV), swinepox virus (SPV), molluscum contagiosum (MCV), yaba monkey tumor virus virus (YMTV), myxoma virus (MYX), and fowlpox virus (FPV).

results indicate that the G7 gene of C*ts*11 contains two mutations which direct distinct amino acid substitutions, either of which are sufficient to impart a temperature-sensitive phenotype.

Retention of the two AG ↓ X sites proteolytic processing in G7 appears to be important for virus viability. The G7 ORF contains two AG ↓ X cleavage sites for proteolytic processing by the viral protease (37), one leading to cleavage at residue 183 and the other at residue 238. We utilized the above described marker rescue protocol to approach the question of whether these sites were essential for virus viability. During marker rescue, the linear, exogenous G7 fragment introduced by transfection must undergo homologous recombination into the endogenous locus in order to generate temperature-insensitive virus. We therefore constructed G7 alleles in which one or both cleavage sites had been altered [G7($_{G183A}$), G7($_{G239A}$), G7($_{G183A;G239A}$)]; the nucleotide substitutions lead to the loss of diagnostic restriction sites as well as causing the desired amino acid substitutions. These altered alleles were introduced into C*ts*11-infected cells in parallel with the wt allele, and temperature-insensitive isolates were plaque purified from each infection/transfection. As shown in Fig. 5, we would predict that generation of these viruses would have required recombination between the genome and the transfected fragment both upstream of the temperature-sensitive mutations in interval 1 and downstream of the temperature-sensitive mutations in intervals 2a (138 nucleotides [nt]), 2b (161 nt), or 2c (399 nt). Depending upon whether recombination had occurred in 2a, 2b, or 2c, the genome would either retain or lose the diagnostic endonuclease sites and associated proteolytic cleavage sites. The genotype of the temperature-insensitive plaques obtained from each transfection was determined: in all cases, the sequences encoding both AG ↓ X cleavage sites were retained (i.e., recombination occurred at 2a or 2b but not within region 2c). We are confident that the temperature-insensitive viruses arose as a consequence of recombination and not reversion, as evidenced by the dramatic difference in the frequency of temperature-insensitive viruses seen upon transfection (see Fig. 4A, rows 1 to 3). These results suggest that cleavage of G7 after amino acids 183 and 238 is important for virus viability.

During nonpermissive C*ts*11 infections, virion production is compromised but the G7 and A30 proteins accumulate normally. The preliminary phenotypic analysis of C*ts*11 is shown in Fig. 6A and B. C*ts*11 showed a very tight temperature-sensitive phenotype, with plaque formation appearing normal at 31.5°C but being completely abrogated at 39.7°C (Fig. 6A). The 24 h viral yield from cells infected with C*ts*11 at nonpermissive temperature was decreased by almost 3 orders of magnitude at an MOI of 2 and by 2.5 orders of magnitude at an MOI 15; the viral yields obtained from wt and C*ts*11 infections performed at 31.5°C were comparable (Fig. 6B).

In many instances the phenotypic defect seen during nonpermissive infections with temperature-sensitive mutants is due to the instability of the mutant protein. Immunoblot analysis of lysates prepared from permissive and nonpermissive C*ts*11 infections was performed to investigate the stability of the G7 protein. Figure 6C (left panel) illustrates that the levels of G7 were comparable during permissive and nonpermissive infections, indicating that the amino acid substitutions cause a loss-of-function rather than a gross misfolding. Under nonpermissive conditions the G7 protein does not undergo proteolytic processing at its internal AG ↓ X sites (25) (Fig. 6C, left panel, compare full-length protein [▲] with processed fragments [△] in samples prepared at 31.5 and 39.7°C), indicative of a block in viral morphogenesis. Previous reports have indicated that the A30 and G7 proteins are mutually dependent upon each other for stability (25), making it impossible to dissect the individual contributions of the two proteins. Because G7 was apparently stable during nonpermissive C*ts*11 infections, we hypothesized that A30 would remain stable as well. As shown in the right panel of Fig. 6C, A30 does indeed accumulate normally during nonpermissive C*ts*11 infections. Thus, this mutant provides the first opportunity to probe the impact of a loss of G7 function without the complication of A30 instability. Further immunoblot analyses (not shown) confirmed that the accumulation of numerous other late proteins was unaffected,

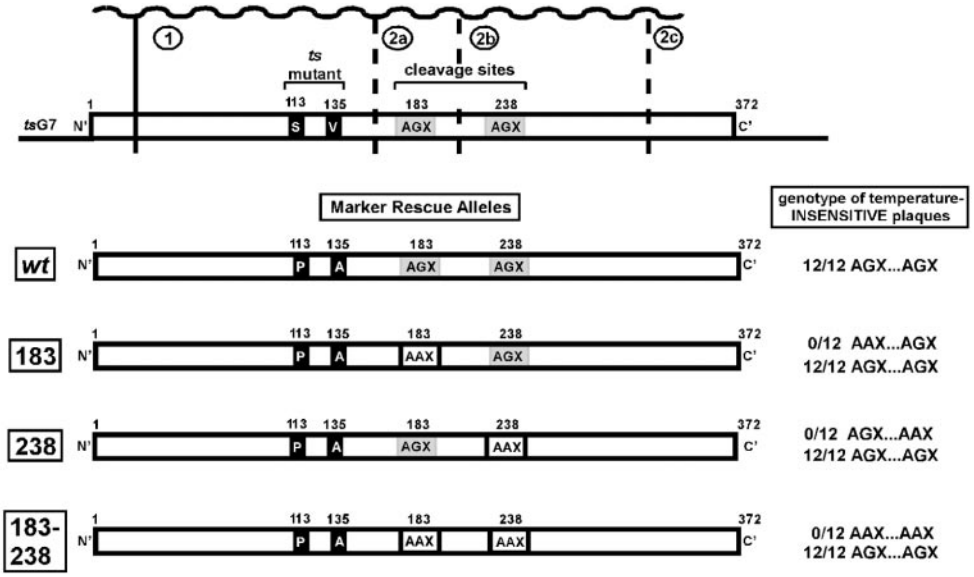

FIG. 5. The AG ↓ X proteolytic cleavage sites within G7 appear to be required for virus viability. Marker rescue analysis was used to assess the requirement for proteolytic cleavage sites found at amino acids 183 and 238 within the G7 protein. Briefly, cells were infected with C*ts*11 at the permissive temperature; they were shifted to the nonpermissive temperature at 3 hpi upon transfection with linearized DNA plasmids encoding wtG7 or mutant alleles engineered to contain nucleotide substitutions which transform one or both AG ↓ X motifs to the inert sequence AAX and, fortuitously, disrupt diagnostic restriction endonuclease sites. Cells were harvested at 48 hpi and 12 temperature-insensitive plaques were purified from each transfection. Homologous recombination between the transfected DNA and the viral genome must occur within interval 1 and either interval 2a, 2b, or 2c in order to generate temperature-insensitive plaques. Depending on whether recombination occurs within 2a, 2b, or 2c, the genome will retain the endogenous AG ↓ X motif (and hence the restriction endonuclease site) or acquire the AAX sequence of the plasmid (and lose the restriction endonuclease site). For each plasmid used, the tally of AG ↓ X versus AAX for the 12 temperature-insensitive plaques obtained from the transfection is shown to the right of the schematic illustration.

establishing that the temperature-sensitive phenotype of C*ts*11 was not a consequence of a disruption in late gene expression.

The C*ts*11-encoded G7 protein shows an impaired ability to associate with A30 in vitro. Both the *ts*G7 and A30 proteins are stable during nonpermissive C*ts*11 infections (Fig. 6C), suggesting that the mutation directly affects the function of G7. Because G7 has been shown to interact with A30 directly, we decided to test whether this property was retained by the

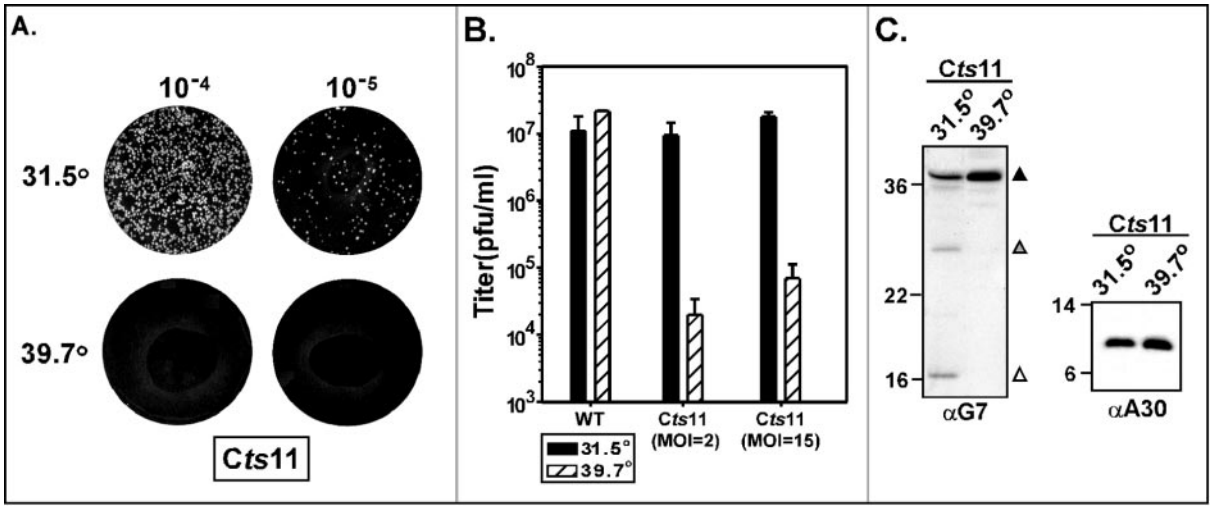

FIG. 6. C*ts*11 displays a tight temperature-sensitive phenotype. (A) Plaque formation by C*ts*11 is abrogated during nonpermissive infections. Serial dilutions of C*ts*11 were titrated at permissive (31.5°C) and nonpermissive (39.7°C) temperatures; at 48 hpi, no macroscopic plaques were seen at 39.7°C. (B) Virus production is drastically reduced during nonpermissive infections with C*ts*11. BSC40 cells were infected (MOI of 2 or 15) with wt virus (■) or C*ts*11 (▨) and maintained at 31.5 or 39.7°C for 24 h. The yield of cell-associated virus was determined by titration at 31.5°C. The values shown represent the average of triplicate experiments. (C) The G7 and A30 proteins are stable during nonpermissive C*ts*11 infections. BSC40 cells were infected with C*ts*11 at 31.5 and 39.7°C (MOI of 5); at 12 hpi, cells were harvested and lysates were subjected to immunoblot analysis with α-G7 (left panel) and α-A30 antisera (right panel). For G7, the immunoreactive bands representing the full-length (▲, 42 kDa) and processed forms (▲, 26 kDa; △, 16 kDa) of G7 are indicated. Note that proteolytic processing of G7 fails to occur at 39.7°C. Molecular weight markers are indicated at the left of each immunoblot, with their masses shown in kilodaltons.

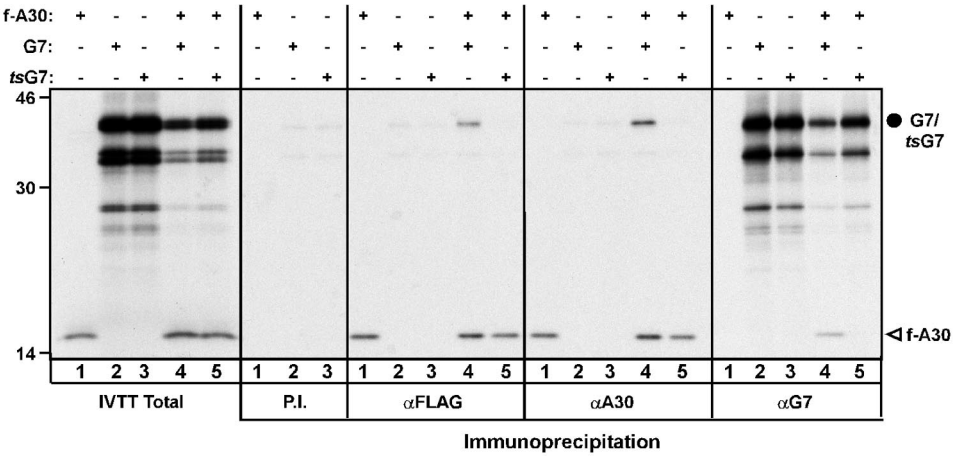

FIG. 7. The C*ts*11-encoded G7 protein shows a diminished ability to interact with the A30 protein in vitro. IVTT reactions were programmed to express 3XFLAG-A30 (F-A30), G7, or C*ts*11-encoded G7 (*ts*G7), either individually or in combination. Total IVTT and the proteins retrieved by immunoprecipitation with preimmune, αFLAG, αA30, or αG7 sera were analyzed by SDS-PAGE and autoradiography. The full-length G7 and *ts*G7 proteins (●) and F-A30 are indicated (△) are indicated, and molecular weight markers are indicated at the left, with their masses shown in kilodaltons. Full-length G7, but not *ts*G7, is coprecipitated by the αA30 or αFLAG sera when F-A30 is present; F-A30 is coprecipitated by the α-G7 serum when G7, but not *ts*G7, is present.

C*ts*11-encoded protein (*ts*G7). The proteins of interest were synthesized using an IVTT protocol, and their interaction was assayed by monitoring coimmunoprecipitation (Fig. 7). The leftmost panel represents a fraction of the total products produced by IVTT: the 3XFLAG-A30 protein is evident (△; F-A30), as are the wt and *ts*G7 proteins (●). In addition to the full-length G7 protein, several smaller species are seen, probably the result of internal initiation or premature termination. No proteins were retrieved when the immunoprecipitation was performed with preimmune serum (lanes 1 to 3; P.I.). The α-FLAG and α-A30 sera retrieved the 3XFLAG-A30 protein but showed no cross-reactivity with either of the G7 proteins (compare lanes 1 with 2,3; αFLAG and αA30). Likewise, the αG7 serum retrieved the G7 proteins but showed no cross-reactivity with the A30 protein (compare lanes 2 and 3 with lane 1; αG7). When 3XFLAG-A30 and wt G7 were cotranslated in IVTT reactions and subjected to immunoprecipitation with α-FLAG, α-A30, or α-G7 sera, the A30 and G7 proteins were coprecipitated in each case (lanes 4; αFLAG, αA30, and αG7). Only the full-length G7 protein was coprecipitated when either the α-FLAG or the α-A30 serum was used (●; compare lanes 4 of the IVTT Total and the αFLAG and αA30 panels), suggesting either that the A30-G7 interaction requires the intact N′ or C′ terminus of G7 or that only the full-length G7 protein assumes the conformation required for protein-protein interaction. In contrast to what we consistently observed for the wt G7 protein, *ts*G7 was not found to coprecipitate with 3XFLAG-A30 when either the α-FLAG, α-A30, or α-G7 sera were used (lanes 5; αFLAG, αA30, and αG7). In sum, these results indicate that the direct interaction between A30 and G7 is impaired by the amino acid substitutions present in the *ts*G7 protein.

Nonpermissive infections performed with C*ts*11 exhibit an early morphogenesis arrest. Examination of the phenotype engendered by the repression of G7 had indicated that it, like its binding partner A30, was required for the attachment of crescent membranes to the viroplasm and for the appropriate maturation of these crescents into the membrane surrounding spheroid immature virions (25). We undertook an electron microscopic analysis of C*ts*11-infected cells to determine whether a comparable or distinct impact on morphogenesis would be seen. Under permissive conditions (31.5°C), C*ts*11-infected cells looked indistinguishable from wt-infected cells, containing normal "smooth" virosomes (V) and all of the stages of developing virions, including crescents (C), immature virions with or without nucleoids (IV and IVN), and intracellular mature virions (IMV) (Fig. 8A). However, under nonpermissive conditions morphogenesis was arrested at an earlier point than had been seen upon G7 repression (25). In many cells we saw only a cleared area of cytoplasm devoid of organelles (Fig. 8B); in some cases, there were several electron-dense, linear structures that might be fibrillar in nature or represent aberrant crescents (△; Fig. 8B and C). In those cells in which virosome formation was apparent, the virosomes had the cur-

FIG. 8. Infections with C*ts*11 at nonpermissive temperature arrest at an early stage in viral morphogenesis. BSC40 cells were infected with Cts11 (MOI of 2) and maintained at either 31.5°C (A) or 39.7°C (B to F); at 17 h, cells were prepared for examination by transmission electron microscopy. All of the normal intermediates of morphogenesis were seen at the permissive temperature (in panel A), including prototypic "smooth" virosomes (V), crescents (C), IV, immature virions with nucleoid (IVN), and IMV. In contrast, cells infected at the nonpermissive temperature (in panels B to F) were devoid of the later stages of virion morphogenesis, as evidenced by the absence of immature or intracellular mature virions. The presence of a cleared area of cytoplasm, with cellular organelles relegated to the cell periphery, was evident in all cells examined (see panel B). Electron-dense fibrillar material was sometimes observed within this cleared area (△; panels B and C). Viral crescents (▲), when observed, were short and clustered within a recognizable but amorphous region of electron-dense material (see panels C, D, and F). These crescent depots were often found near virosomes that displayed a "curdled" appearance (CV; panels C, D, and E). Nuclei are labeled with N. Magnifications: (A) ×30,000; (B) ×12,000; (C) ×30,000; (D) ×32,000; (E) ×40,000; (F) ×48,000. Bars, 500 nm.

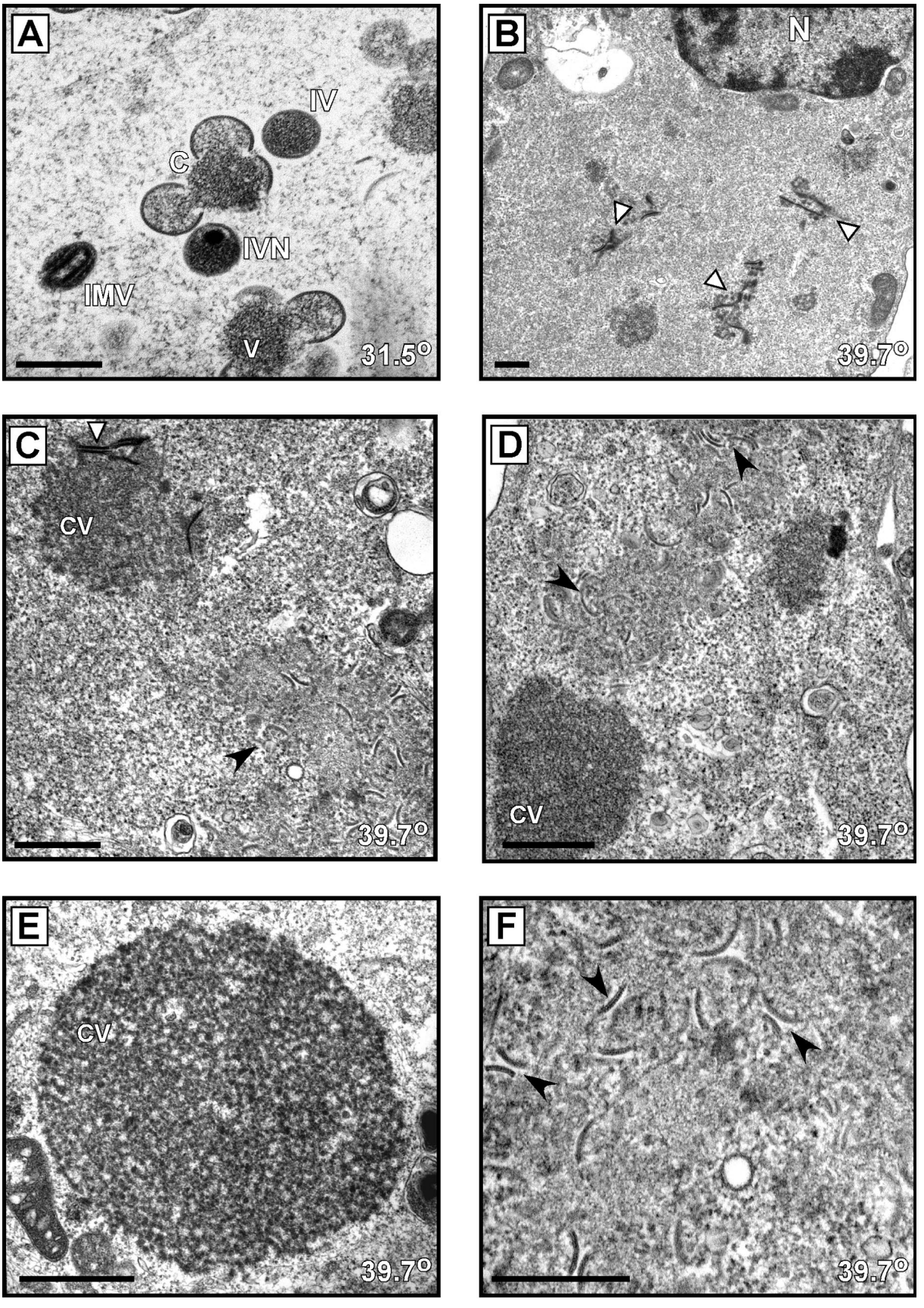
A
IV
C
IVN
IMV
V
31.5°
B
N
39.7°
C
CV
39.7°
D
CV
39.7°
E
CV
39.7°
F
39.7°

dled appearance (CV) seen in cells infected at high temperature with *ts*H5-4, D*ts*46, and vA30Li (Fig. 8C, D, and E) (6, 27, 30). Short crescents were observed in a minority of cells but appeared in clusters which were embedded in an electron-dense matrix (Fig. 8C, D, and F). We have not observed such crescent depots during our analyses of wt morphogenesis. This analysis has uncovered an additional role for the G7 protein in the assembly of normal virosomes; this role is distinct from the prior observation that G7 and A30 together are important for the maturation of crescents and the establishment of crescent-virosome interactions.

Execution point analysis indicates that the mutation in C*ts*11 also exerts an affect after the rifampin-sensitive step in virion morphogenesis. A caveat to the study of temperature-sensitive mutants is that, by definition, the phenotype seen reflects the first lethal consequence of incubation under nonpermissive conditions. Any subsequent impact that inactivation of the protein of interest would have is, de facto, obscured. Upon determination that the arrest seen in nonpermissive C*ts*11 infections was at an earlier stage of morphogenesis than had been seen upon repression of G7 (25), we hypothesized that the G7 protein might be required for multiple stages of virion maturation. As an approach to investigating this possibility, we performed a series of RIF release experiments that we have used successfully to elucidate the functions of the A13 and F10 proteins (10, 33). Briefly, four sets of wt- and C*ts*11-infected cells were maintained at 31.5°C in the presence of RIF. At 12 hpi, the sets were subjected to different treatments (Fig. 9A). Two sets were maintained at 31.5°C; one was left in the presence of drug, and one was washed and refed with medium lacking drug (RIF release). Two additional sets were shifted to 39.7°C (shift); again, one set was left in the presence of drug, whereas one was washed and refed with medium lacking drug. Cells were harvested after an additional 7 h of incubation; the viral yield was determined by serial titration, and the integrity and processing of the G7 protein was determined by immunoblot analysis (Fig. 9A). When cultures were maintained at 31.5°C, virus production resumed after RIF release in both wt- and C*ts*11-infected cells: released cultures produced 100-fold more infectious virus than cultures maintained in the presence of drug (compare 1 and 2). In cultures shifted to 39.7°C, however, only the wt infections recovered from the RIF release and demonstrated a burst in viral production; no recovery was seen in C*ts*11-infected cultures (compare 3 and 4). These data indicate C*ts*11 has an execution point that is later than the RIF-sensitive step in morphogenesis. Immunoblot analysis revealed that G7 accumulated to equivalent levels under all of these conditions; proteolytic processing, however, was strictly correlated with the resumption of virus production (shaded and open triangles; lanes 3, 4, and 7).

Having shown that the production of infectious virus did not resume when C*ts*11-infected cultures were shifted to 39.7°C at the time of drug removal, we wanted to examine the stage of morphogenesis at which these cultures arrested. Again, cells were infected with wt or C*ts*11 virus in the presence of RIF and maintained at 31.5°C. At 12 hpi, one set (wt and C*ts*11) of dishes was processed for EM analysis (no RIF release; panels 1, 2, 5, and 6); a second set of dishes was washed, refed with medium lacking RIF, and shifted to 39.7°C for an additional 3 h of incubation (Shift/RIF release; panels 3, 4, and 7 to 10) prior to being processed for EM analysis. After 12 h of infection at 31.5°C In the presence of RIF, both wt- and C*ts*11-infected cultures exhibited the classic rifampin block (19): virosomes (V) surrounded by flaccid membranes, DNA crystalloids, but no IV, IVN, or IMV (Fig. 9B, panels 1, 2, 5, and 6). When wt-infected cells were shifted to 39.7°C and released from the RIF arrest, morphogenesis resumed and the cells possessed all of the hallmarks of normal morphogenesis, including crescents (C) adjacent to virosomes (V), IV, and clusters of infectious IMV (panels 3 and 4). To the contrary, upon temperature shift and withdrawal of RIF from C*ts*11-infected cells, viral morphogenesis appeared to resume and then arrest again with the appearance of numerous clusters of isolated crescents (C), curdled virosomes (CV), and aberrant, empty IV (◇; panels 7 to 10). Some of these aberrant IV contained a central patch of viroplasm that failed to make contact with the membrane; many appeared to contain internal vesicles or tubules (△; panels 8 to 10). This phenotype was remarkably similar to that which had been seen upon repression of G7 or A30 or during nonpermissive infections with the *ts*A30 virus (vG7Li, vA30Li, and D*ts*46) (25, 27, 30). In sum, manipulation of G7 expression or function using the inducible or tempera-

FIG. 9. Rifampin release experiments reveal a second block for nonpermissive C*ts*11 infections at a later stage of viral morphogenesis. (A) C*ts*11 is unable to recover from a RIF block at the nonpermissive temperature. Quadruplicate sets of BSC40 cells were infected (MOI of 5) with either wt virus (■) or C*ts*11 (▨) at 31.5°C in the presence of RIF. At 12 hpi two sets of wt and C*ts*11 infections were left at 31.5°C (rows 1 and 2) and two sets were shifted to 39.7°C (rows 3 and 4); 1 set at each temperature was released from the RIF block (striped bar, rows 2 and 4); the other set was maintained in the presence of drug (rows 1 and 3). Infections were then allowed to proceed for an additional 7 h; the viral yield was determined by titration at 31.5°C in triplicate, and the averaged results are displayed graphically. Unlike wt-infected cells, C*ts*11-infected cells only resumed virus production when RIF release was performed at 31.5°C. Samples from these infections were also subjected to immunoblot analysis with α-G7 serum (right panel). The immunoreactive species corresponding to full-length (solid triangles) and cleaved G7 (shaded and open triangles) are indicated, and the molecular mass markers are shown at the left in kilodaltons. Processing of G7 was correlated with recovery of virus production. (B) After RIF release at 39.7°C, the morphogenesis arrest seen in C*ts*11-infected cultures is reminiscent of that seen upon repression of G7 expression. Duplicate sets of BSC40 cells were infected (MOI of 5) with either wt virus or C*ts*11 in the presence of RIF and maintained at 31.5°C. At 12 hpi 1 set was harvested for EM analysis; the classic features of the morphogenesis arrest associated with RIF treatment were seen in both wt- and C*ts*11-infected cells (compare panels 1 and 2 and panels 5 and 6). A second set was shifted to 39.7°C, released from the RIF block, and incubated for an additional 3 h (compare panels 3 and 4 to panels 7 to 10). In wt-infected cells, morphogenesis resumed and progressed normally, culminating with the formation of mature virions. In C*ts*11-infected cells, there was a release from the RIF arrest, but a second arrest was seen, with the appearance of numerous crescents and empty or pseudo-immature virions. The latter were often found to include what appear to be vesicles. There was a complete absence of immature or mature virions. Abbreviations are as follows: virosome (V), crystalloids (→), viral crescents (C), IV, IMV, curdled virosome (CV), pseudo-IV (◇), and vesicles (△). Subpanel magnifications: 1, ×17,500; 2, ×30,000; 3, ×10,000; 4, ×28,000; 5, ×33,000; 6, ×33,000; 7, ×11,500; 8, ×30,000; 9, ×60,000; 10, ×34,000. Bars, 500 nm.

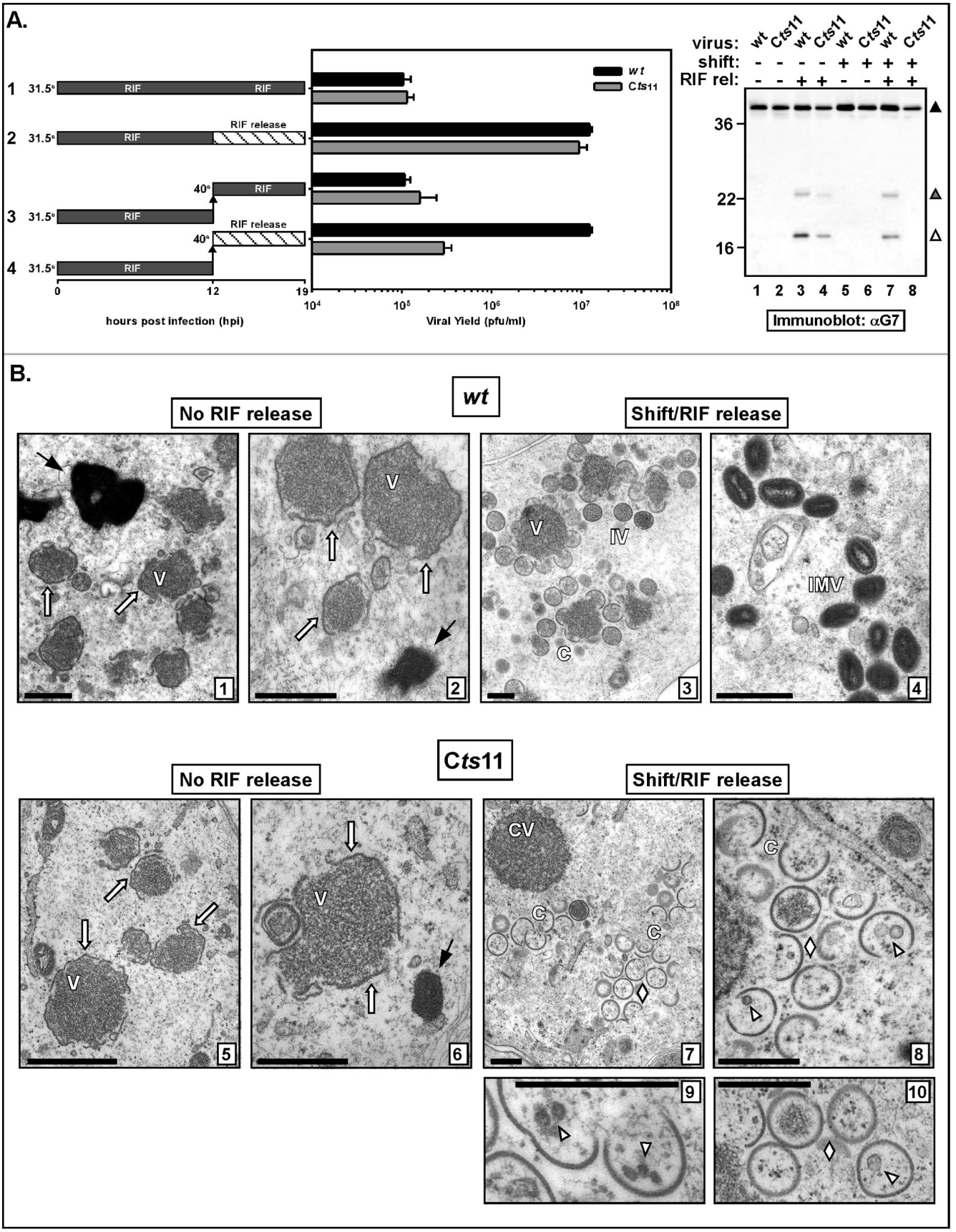
A.
1 31.5° RIF RIF
2 31.5° RIF RIF release
3 40° RIF 31.5° RIF
4 40° RIF release 31.5° RIF
0 12 19
hours post infection (hpi)
wt
Cts11
10^4 10^5 10^6 10^7 10^8
Viral Yield (pfu/ml)
virus: wt Cts11 wt Cts11 wt Cts11 wt Cts11
shift: - - - - + + + +
RIF rel: - - + + - - + +
36
22
16
1 2 3 4 5 6 7 8
Immunoblot: αG7
B.
wt
No RIF release
Shift/RIF release
V
IV
C
IMV
1 2 3 4
Cts11
No RIF release
Shift/RIF release
V
CV
C
5 6 7 8 9 10

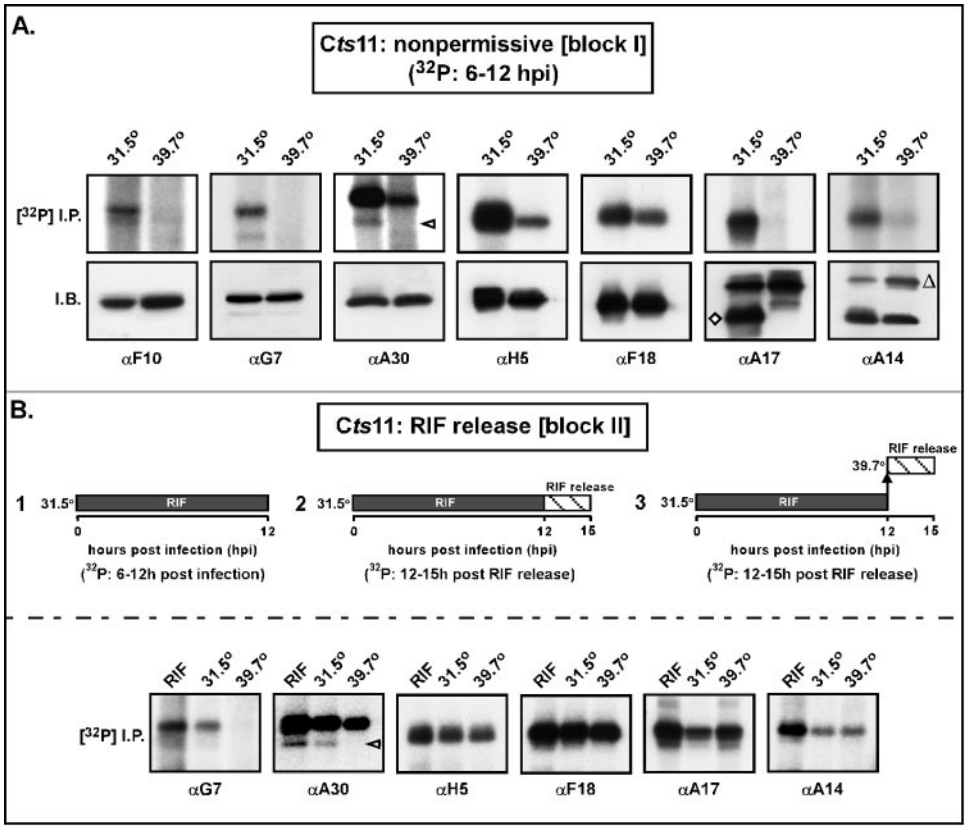

FIG. 10. During nonpermissive C*ts*11 infections, the phosphorylation of several viral proteins involved in morphogenesis is impaired. (A) Comparison of protein phosphorylation during C*ts*11 infections performed at 31.5°C versus 39.7°C. BSC40 cells were infected with C*ts*11 (MOI of 5) at either the permissive (31.5°C) or nonpermissive (39.7°C) temperature and metabolically labeled with ^{32}PPi from 6 to 12 hpi. Cell lysates were subjected to immunoprecipitation analysis with a variety of antisera (αF10, αG7, αA30, αH5, αF18, αA17, and αA14); immunoprecipitates were resolved by SDS-PAGE and visualized by autoradiography ([^{32}P]I.P.; top panels). In parallel, lysates were also subjected to immunoblot analyses with the indicated antisera to confirm and quantitate the presence of the relevant proteins (I.B.; bottom panels). Phosphorylation of F10, G7, A30 (▷), A17, and A14 was barely detectable at the nonpermissive temperature; significant reduction in the phosphorylation of H5 and modest reduction in the phosphorylation of F18 was also observed. Comparable accumulation of all of the proteins was observed at both temperatures; at 39.7°C, however, processing of A17 (◇) failed to occur, and elevated levels of glycosylated A14 (△) were seen. (B) Comparison of protein phosphorylation during C*ts*11 infections maintained in the presence of RIF or released from RIF arrest at 31.5 or 39.7°C. BSC40 cells were infected with C*ts*11 (MOI of 5) in triplicate in the presence of RIF. One plate was metabolically labeled with ^{32}PPi from 6 to 12 hpi and then harvested. The other two plates were released from the RIF block at 12 hpi and maintained at either 31.5 or 39.7°C for 3 h in the presence of ^{32}PPi before being harvested. The cell lysates were analyzed as described above for panel A. Under these conditions, the phosphorylation of A14, A17, F18, and H5 were comparable at both temperatures; however, as in panel A, no phosphorylation of A30 or G7 was observed at 39.7°C.

ture-sensitive viruses suggests that G7 is involved at several stages of infection that occur both prior to and after the RIF-sensitive step of morphogenesis.

F10 kinase-dependent phosphorylation of several substrates is abrogated during Cts11 infections performed at the nonpermissive temperature. During ongoing morphogenesis, a number of viral proteins are modified by F10-mediated phosphorylation and/or proteolytic processing. Repression of the A30 and/or G7 protein has been proposed to interfere with the stability and/or activity of the F10 kinase (29). We therefore monitored the phosphorylation status and steady-state levels of F10 and several other viral proteins (G7, A30, H5, F18, A17, and A14) in the context of a nonpermissive C*ts*11 infection (Fig. 10A). Cells were infected with C*ts*11 at the permissive (31.5°C) and nonpermissive (39.7°C) temperatures and metabolically labeled with ^{32}PPi from 3 to 12 hpi; lysates were subjected to immunoblotting and immunoprecipitation analysis with αF10, αG7, αA30, αH5, αF18, αA17, and αA14 sera. Phosphorylation of the F10 kinase itself, which is presumed to reflect autophosphorylation, was abrogated in the context of a nonpermissive C*ts*11 infection, although the level of protein accumulated was not reduced (Fig. 10A; αF10). Several of the viral proteins known to be F10 substrates displayed diminished (H5 and F18) or undetectable (G7, A30, A14, and A17) levels of [^{32}P] incorporation during the 39.7°C C*ts*11 infection (upper panels). Protein accumulation was not affected, confirming that the data reflect true changes in the phosphorylation status of these proteins (lower panels).

This analysis was also extended to C*ts*11-infected cultures that had been maintained at 31.5°C in the presence of RIF for 12 h and then harvested directly or released from the RIF block and incubated for an additional 3 h at either 31.5°C or 39.7°C (Fig. 10B). Cells were metabolically labeled with ^{32}PPi either from 6 to 12 hpi (during RIF arrest) or from 12 to 15 hpi (after RIF release). Ongoing phosphorylation of A14, A17, H5, F18, A30, and G7 was observed at 31.5°C in the presence

of RIF (left lanes). Likewise, continued phosphorylation of these proteins was observed when the cultures were released from RIF and maintained at 31.5°C (middle lanes). However, a different profile was seen when the cultures were shifted to 39.7°C upon release from the RIF arrest (right lanes). Continued phosphorylation of A14, A17, H5, and F18 was observed, but no ongoing phosphorylation of A30 or G7 could be detected. Apparently, either the conformation or spatial organization of these proteins is not appropriate for phosphorylation at 39.7°C. These data suggest that the phosphorylation of A14 and A17 requires different temporal and/or spatial conditions than does the phosphorylation of A30 and G7.

DISCUSSION

As more genetic analyses of vaccinia virus morphogenesis are completed, phenotypic patterns emerge that may elucidate the dynamic networks of protein-protein interactions that drive this process. Similarities in the arrests observed upon the repression or inactivation of the A14 membrane protein and the A30, G7, and H5 proteins stimulated the studies described here. Perturbations in A14, A30, and G7 disrupt virosome-crescent association (24, 25, 27, 30, 32); because of our prior interest in the A14 protein, we were interested in probing whether interactions between these three proteins might bring virosomes and crescents together. Defects in A30, G7, and H5 affect the integrity of the virosomal matrix at high temperature, rendering them "curdled" or "lacy" (6, 27, 30); because of our prior interest in the H5 protein, we were interested in determining whether a common mechanism was responsible for undermining virosomal integrity.

Using a variety of antisera directed against these proteins, we were unable to detect any physical interaction between A14 and either A30 or G7. Although such negative data are not definitive, they suggest that the association of virosomes with crescents is not mediated by formation of an A30/G7/A14 complex. We did consistently detect an interaction between the A30 protein and the F18 protein, a highly abundant virion component (11). Although it remains to be determined whether there is any functional significance to this apparent interaction, both proteins have been found within virosomes and are encapsidated within virions, localizing at the core-membrane boundary (30, 32).

Our lab has been interested in the role of reversible protein phosphorylation in the vaccinia virus life cycle and, more specifically, in the role of the virus-encoded F10 kinase in orchestrating morphogenesis (31) and the H1 phosphatase in enabling virion infectivity (16). We therefore analyzed the possible phosphorylation of the A30 and G7 proteins during infection. Both A30 and G7 are phosphorylated on *ser* residues during infection in a manner that is genetically dependent upon the F10 kinase and/or on ongoing morphogenesis. F10-dependent phosphorylation of A30 was also demonstrated by Szajner et al. (29) during the course of our studies. We have also shown that purified A30 protein is an effective substrate for both the vaccinia virus F10 and B1 kinases in vitro; identification of the site(s) of phosphorylation and the biological importance of this modification will be the subject of future work. Interestingly, the G7 protein, either alone or in the presence of A30, did not serve as a substrate for either the F10 or B1 protein kinase in vitro. It may be that G7 is phosphorylated by a cellular kinase in vivo or that phosphorylation by a viral kinase only occurs within the intracellular context of ongoing morphogenesis.

Previous studies have demonstrated that the A30 and G7 proteins are mutually dependent upon one another for their stability (25). Interestingly, we found that their stability was also dependent upon the presence of a functional H5 protein. These data suggest that the loss of A30 and/or G7 may underlie the virosomal curdling observed in *ts*H5 infections (6). The relationship between A30 and G7 was not reciprocal, since we observed no change in the steady-state levels of H5 during nonpermissive infections performed with either Dts46 (*ts*A30) or C*ts*11 (*ts*G7) (not shown). H5 has not been found to be associated with the multiprotein complex comprised of A30, G7, F10, J1, D2, D3, and A15 (26). Since nonpermissive *ts*H5 infections arrest at an earlier stage than do infections in which A30 or G7 are repressed or impaired, it is possible that the abundant H5 protein provides a matrix within which the multiprotein complex forms and within which F10 can direct the phosphorylation of core components.

During the course of these studies, the preliminary mapping of two temperature-sensitive mutants (C*ts*11 and C*ts*41) to the genomic interval comprising the G6R, G7L, and G8R genes was reported in an overall compilation of the available collections of temperature-sensitive mutants (14). We obtained both of these mutants and analyzed them for plaque formation and 24 h viral yield under permissive and nonpermissive conditions. Both viruses were temperature sensitive for 24 h yield, whereas C*ts*41 was determined to be leaky by plaque assay, forming small plaques at the nonpermissive temperature. We therefore chose to pursue a genotypic and phenotypic analysis of C*ts*11. Our determination that the C*ts*11 G7 gene contains two lesions that each appear to contribute to temperature sensitivity may explain the very tight conditional lethal phenotype of this virus. The *ts*G7 protein was stable at 39.7°C, as was its binding partner, A30. For the first time, therefore, we had a tool to dissect the function of G7 without the accompanying loss of A30. EM analysis of nonpermissive C*ts*11 infections revealed that viral morphogenesis arrested at an earlier stage than had been seen previously upon repression of G7 expression. Many cells contained only a cleared area of cytoplasm, which sometimes contained linear fragments of what appeared to be membranous material; others displayed curdled virosomes or unusual electron dense zones within which were found numerous membrane crescents. These images were quite distinct from what had been observed upon repression of G7; in this case, morphogenesis progressed to the formation of what appeared to be empty or multiply wrapped immature virions.

There are several distinctions between temperature-sensitive mutants and inducible recombinants: the presence of a stable but nonfunctional protein is quite distinct from the presence of only trace amounts of a wild-type protein. Whereas the stability of the A30 protein during C*ts*11 infections might have been predicted to lead to a milder phenotype than that observed upon the loss of both G7 and A30, it is also reasonable to hypothesize that low amounts of wt G7 protein might be more effective at performing some G7-dependent functions than would substantial amounts of the inactive *ts*G7 protein. We therefore considered it likely that G7 played multiple roles

in viral morphogenesis and so performed execution point studies to identify temperature-sensitive stages that were downstream of the arrest induced by rifampin. Unlike wt-infected cultures, C*ts*11-infected cultures were only able to recover when they were maintained at 31.5°C after release from the rifampin block. If they were shifted to 39.7°C upon release from rifampin, no burst of infectious virus was produced, and EM analysis indicated that morphogenesis arrested at a stage comparable to that seen upon repression of G7. Numerous empty immature virions were seen, some of which contained internal patches of viroplasm or vesicles. These data indicate that a functional G7 protein is required for several stages of viral morphogenesis: first, in the establishment and integrity of virosomes and crescents and later for the envelopment of the viroplasm by the maturing crescent. Interestingly, the block seen when RIF-arrested cultures were released from drug at 39.7°C is quite similar to that which we observe when *ts*F10 cultures are subjected to the same regimen (20), suggesting that the interactions between F10, G7, and A30 may be extremely important for the incorporation of viroplasm into nascent IV.

The G7 protein encoded by C*ts*11 appears to be stable but nonfunctional at the nonpermissive temperature. Although function per se is difficult to test in the absence of enzymatic activity, a physical interaction between G7 and A30 has been documented. We cannot detect this interaction when our α-G7 and α-A30 antisera are used in immunoprecipitation analyses of infected extracts. As an alternative approach, we made use of a coupled IVTT system to test the binary interaction between 3XFLAG-A30 (F-A30) and either G7 or *ts*G7. When F-A30 and wt G7 were cotranslated, their direct interaction could be readily confirmed by coimmunoprecipitation with α-FLAG, α-A30, or α-G7 sera. However, no such interaction between F-A30 and *ts*G7 could be detected. The two amino acid substitutions (Pro→Ser and Ala→Val) within *ts*G7 abrogate the A30/G7 interaction in vitro; by extrapolation, we propose that they also weaken the interaction in vivo in a manner that compromises ongoing morphogenesis.

Because A30 and G7 are both phosphorylated in vivo in a manner that is dependent upon the presence of a functional F10 kinase, we wanted to investigate the phosphorylation profile of key viral proteins during nonpermissive C*ts*11 infections. When such infections are initiated and maintained at 39.7°C, phosphorylation of A14, A17, F10, A30, and G7 was abrogated, and phosphorylation of H5 and F18 was diminished. Because the F10 protein remained stable under these experimental conditions, this observation supports a model wherein F10-mediated phosphorylation is linked to ongoing morphogenesis. The appropriate kinase-substrate interactions may only occur within the spatial context of assembly intermediates.

This approach was also used to analyze the phosphorylation status of wt and C*ts*11 infections maintained for 12 h at 31.5°C in the presence of RIF; under these circumstances, appropriate phosophorylation of A14, A17, A30, G7, H5, and F18 was observed when ^{32}PPi was present from 6 to 12 hpi. When similarly infected cultures were then released from the RIF block and maintained for an additional 3 h at 31.5 or 39.7°C in the presence of ^{32}PPi, a different picture emerged. Ongoing phosphorylation of all of the proteins tested was observed at 31.5°C. However, although phosphorylation of A14, A17, H5, and F18 continued at 39.7°C, no further phosphorylation of

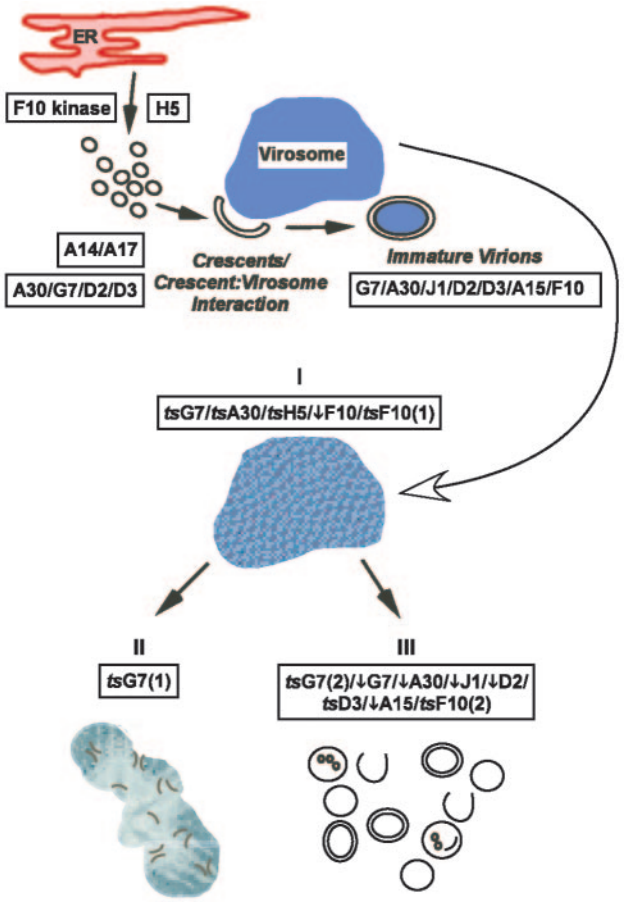

FIG. 11. Working model of early stages in VV morphogenesis. The formation of virosomes, crescents, and immature virions is shown schematically; the proteins implicated in the various stages are listed within the black boxes. The curved arrow leads to aberrant features seen when the proteins indicated are repressed (↓) or impaired (*ts*): I, curdled virosomes; II, crescent depots; III, empty, pseudo-IV. Depending on the experimental regimen, *ts*F10 and *ts*G7 show two different arrests [(1) and (2)].

A30 or G7 was observed at the high temperature. This deficit in phosphorylation was accompanied by the formation of empty immature virions that had failed to engulf virosomal contents. Cumulatively, these data indicate that the amino acid substitutions within the *ts*G7 protein alter the interactions between A30 and G7, prevent the phosphorylation of G7, and its binding partner A30 at 39.7°C, and prevent the enclosure of virosomal contents within emerging IV. In the future, it will be important to establish which of these deficits is primary and which secondary, to define the sites of phosphorylation on the A30 and G7 proteins, and to clarify which kinase is directly responsible for phosphorylating G7 in vivo.

During morphogenesis, the G7 protein undergoes proteolytic processing as well as phosphorylation. To test the importance of this proteolytic processing, we performed marker rescue analysis with alleles in which neither, one, or both of the AG ↓ X cleavage sites was disrupted. Based on the size of the DNA intervals available for homologous recombination, incorporation of the disrupted sites would have been favored if the inability to undergo cleavage did not compromise virus viability. However, none of the 12 plaques analyzed from each res-

cue experiment contained disrupted AG↓X sites, strongly suggesting that the ability of G7 to undergo processing is highly favored. The processing of G7 occurs after the RIF-sensitive step of morphogenesis (Fig. 9A, lanes 1 and 2); by extrapolation from other studies, it is likely that this processing is not required for the inclusion of viroplasm into IV but for the subsequent IV→IMV transition.

In sum these studies have extended our understanding of the roles played by the A30 and G7 proteins during the viral life cycle and of the functional interactions between A30, G7, H5, and F10. Figure 11 incorporates these findings into a schematic view of the early events of virion assembly. Through various functional and physical interactions, all of these proteins participate in the formation of virosomes and the incorporation of virosomal contents into nascent immature virions (4, 6, 20, 23–27, 29–32, 36). Further dissection of this process should enhance our understanding of how protein phosphorylation facilitates the rapid and accurate assembly of large macromolecular complexes such as vaccinia virions.

ACKNOWLEDGMENTS

This study was supported by a grant to P.T. by the NIH (2 R01 GM53601).

We thank R. Rock and B. Rohl for generating the α-A30 and α-G7 sera, respectively, and Clive Wells for assistance in preparing the samples for electron microscopy. We thank Mira Punjabi for sharing purified 3X-Flag F10 and for assistance with kinase reactions, R. Jeremy Nichols for sharing purified His-B1 kinase, and the members of the Traktman lab for helpful discussions throughout the preparation of the manuscript.

REFERENCES

1. **Banham, A. H., and G. L. Smith.** 1992. Vaccinia virus gene B1R encodes a 34-kDa serine/threonine protein kinase that localizes in cytoplasmic factories and is packaged into virions. Virology **191:**803–812.
2. **Beaud, G., R. Beaud, and D. P. Leader.** 1995. Vaccinia virus gene H5R encodes a protein that is phosphorylated by the multisubstrate vaccinia virus B1R protein kinase. J. Virol. **69:**1819–1826.
3. **Black, E. P., N. Moussatche, and R. C. Condit.** 1998. Characterization of the interactions among vaccinia virus transcription factors G2R, A18R, and H5R. Virology **245:**313–322.
4. **Chiu, W. L., and W. Chang.** 2002. Vaccinia virus J1R protein: a viral membrane protein that is essential for virion morphogenesis. J. Virol. **76:**9575–9587.
5. **Dales, S., and E. H. Mosbach.** 1968. Vaccinia as a model for membrane biogenesis. Virology **35:**564–583.
6. **DeMasi, J., and P. Traktman.** 2000. Clustered charge-to-alanine mutagenesis of the vaccinia virus H5 gene: isolation of a dominant, temperature-sensitive mutant with a profound defect in morphogenesis. J. Virol. **74:**2393–2405.
7. **Dubochet, J., M. Adrian, K. Richter, J. Garces, and R. Wittek.** 1994. Structure of intracellular mature vaccinia virus observed by cryoelectron microscopy. J. Virol. **68:**1935–1941.
8. **Fuerst, T. R., E. G. Niles, F. W. Studier, and B. Moss.** 1986. Eukaryotic transient-expression system based on recombinant vaccinia virus that synthesizes bacteriophage T7 RNA polymerase. Proc. Natl. Acad. Sci. USA **83:**8122–8126.
9. **Griffiths, G., N. Roos, S. Schleich, and J. K. Locker.** 2001. Structure and assembly of intracellular mature vaccinia virus: thin-section analyses. J. Virol. **75:**11056–11070.
10. **Grubisha, O., and P. Traktman.** 2003. Genetic analysis of the vaccinia virus I6 telomere-binding protein uncovers a key role in genome encapsidation. J. Virol. **77:**10929–10942.
11. **Kao, S. Y., and W. R. Bauer.** 1987. Biosynthesis and phosphorylation of vaccinia virus structural protein VP11. Virology **159:**399–407.
12. **Klemperer, N., J. Ward, E. Evans, and P. Traktman.** 1997. The vaccinia virus I1 protein is essential for the assembly of mature virions. J. Virol. **71:**9285–9294.
13. **Koerner, T. J., J. E. Hill, A. M. Myers, and A. Tzagoloff.** 1991. High-expression vectors with multiple cloning sites for construction of *trpE* fusion genes: pATH vectors. Methods Enzymol. **194:**477–490.
14. **Lackner, C. A., S. M. D'Costa, C. Buck, and R. C. Condit.** 2003. Complementation analysis of the Dales collection of vaccinia virus temperature-sensitive mutants. Virology **305:**240–259.
15. **Lin, S., W. Chen, and S. S. Broyles.** 1992. The vaccinia virus B1R gene product is a serine/threonine protein kinase. J. Virol. **66:**2717–2723.
16. **Liu, K., B. Lemon, and P. Traktman.** 1995. The dual-specificity phosphatase encoded by vaccinia virus, VH1, is essential for viral transcription in vivo and in vitro. J. Virol. **69:**7823–7834.
17. **Mercer, J., and P. Traktman.** 2003. Investigation of structural and functional motifs within the vaccinia virus A14 phosphoprotein, an essential component of the virion membrane. J. Virol. **77:**8857–8871.
18. **Moss, B.** 2001. Poxviridae: the viruses and their replication, p. 2849–2884. *In* D. M. Knipe and P. M. Howley (ed.), Fields virology, 4th ed. Lippincott-Raven Publishers, Philadelphia, Pa.
19. **Moss, B., E. N. Rosenblum, E. Katz, and P. M. Grimley.** 1969. Rifampicin: a specific inhibitor of vaccinia virus assembly. Nature **224:**1280–1284.
20. **Punjabi, A., and P. Traktman.** 2005. Cell biological and functional characterization of the vaccinia virus F10 kinase: implications for the mechanism of virion morphogenesis J. Virol. **79:**2171–2190.
21. **Rempel, R. E., M. K. Anderson, E. Evans, and P. Traktman.** 1990. Temperature-sensitive vaccinia virus mutants identify a gene with an essential role in viral replication. J. Virol. **64:**574–583.
22. **Rempel, R. E., and P. Traktman.** 1992. Vaccinia virus B1 kinase: phenotypic analysis of temperature-sensitive mutants and enzymatic characterization of recombinant proteins. J. Virol. **66:**4413–4426.
23. **Rodriguez, D., M. Esteban, and J. R. Rodriguez.** 1995. Vaccinia virus A17L gene product is essential for an early step in virion morphogenesis. J. Virol. **69:**4640–4648.
24. **Rodriguez, J. R., C. Risco, J. L. Carrascosa, M. Esteban, and D. Rodriguez.** 1998. Vaccinia virus 15-kilodalton (A14L) protein is essential for assembly and attachment of viral crescents to virosomes. J. Virol. **72:**1287–1296.
25. **Szajner, P., H. Jaffe, A. S. Weisberg, and B. Moss.** 2003. Vaccinia virus G7L protein Interacts with the A30L protein and is required for association of viral membranes with dense viroplasm to form immature virions. J. Virol. **77:**3418–3429.
26. **Szajner, P., H. Jaffe, A. S. Weisberg, and B. Moss.** 2004. A complex of seven vaccinia virus proteins conserved in all chordopoxviruses is required for the association of membranes and viroplasm to form immature virions. Virology **330:**447–459.
27. **Szajner, P., A. S. Weisberg, and B. Moss.** 2001. Unique temperature-sensitive defect in vaccinia virus morphogenesis maps to a single nucleotide substitution in the A30L gene. J. Virol. **75:**11222–11226.
28. **Szajner, P., A. S. Weisberg, and B. Moss.** 2004. Evidence for an essential catalytic role of the F10 protein kinase in vaccinia virus morphogenesis. J. Virol. **78:**257–265.
29. **Szajner, P., A. S. Weisberg, and B. Moss.** 2004. Physical and functional interactions between vaccinia virus F10 protein kinase and virion assembly proteins A30 and G7. J. Virol. **78:**266–274.
30. **Szajner, P., A. S. Weisberg, E. J. Wolffe, and B. Moss.** 2001. Vaccinia virus A30L protein is required for association of viral membranes with dense viroplasm to form immature virions. J. Virol. **75:**5752–5761.
31. **Traktman, P., A. Caligiuri, S. A. Jesty, K. Liu, and U. Sankar.** 1995. Temperature-sensitive mutants with lesions in the vaccinia virus F10 kinase undergo arrest at the earliest stage of virion morphogenesis. J. Virol. **69:**6581–6587.
32. **Traktman, P., K. Liu, J. DeMasi, R. Rollins, S. Jesty, and B. Unger.** 2000. Elucidating the essential role of the A14 phosphoprotein in vaccinia virus morphogenesis: construction and characterization of a tetracycline-inducible recombinant. J. Virol. **74:**3682–3695.
33. **Unger, B., and P. Traktman.** 2004. Vaccinia virus morphogenesis: A13 phosphoprotein is required for assembly of mature virions. J. Virol. **78:**8885–8901.
34. **Vanslyke, J. K., C. A. Franke, and D. E. Hruby.** 1991. Proteolytic maturation of vaccinia virus core proteins: identification of a conserved motif at the N termini of the 4b and 25K virion proteins. J. Gen. Virol. **72**(Pt. 2)**:**411–416.
35. **Vanslyke, J. K., S. S. Whitehead, E. M. Wilson, and D. E. Hruby.** 1991. The multistep proteolytic maturation pathway utilized by vaccinia virus P4a protein: a degenerate conserved cleavage motif within core proteins. Virology **183:**467–478.
36. **Wang, S., and S. Shuman.** 1995. Vaccinia virus morphogenesis is blocked by temperature-sensitive mutations in the F10 gene, which encodes protein kinase 2. J. Virol. **69:**6376–6388.
37. **Whitehead, S. S., and D. E. Hruby.** 1994. Differential utilization of a conserved motif for the proteolytic maturation of vaccinia virus proteins. Virology **200:**154–161.
38. **Wolffe, E. J., D. M. Moore, P. J. Peters, and B. Moss.** 1996. Vaccinia virus A17L open reading frame encodes an essential component of nascent viral membranes that is required to initiate morphogenesis. J. Virol. **70:**2797–2808.
39. **Zhang, Y. F., and B. Moss.** 1991. Vaccinia virus morphogenesis is interrupted when expression of the gene encoding an 11-kilodalton phosphorylated protein is prevented by the *Escherichia coli* lac repressor. J. Virol. **65:**6101–6110.